Dalton Transactions

Accepted Manuscript

ROYAL SOCIETY OF CHEMISTRY

www.rsc.org/dalton

Synthesis, X-ray structure and *in vitro* cytotoxicity studies of Cu(I/II) complexes of thiosemicarbazone: Special emphasis on their interactions with DNA

Saswati Bhakat,[a] Ayon Chakraborty,[b] Subhashree P. Dash,[a] Alok K. Panda,[b] Rama Acharyya,[a]* Ashis Biswas,[b] Subhadip Mukhopadhyay,[c] Sujit K. Bhutia,[c] Aurélien Crochet,[d] Yogesh P. Patil,[e] M. Nethaji[e] and Rupam Dinda[a]*

[a]*Department of Chemistry, National Institute of Technology, Rourkela 769008, Odisha, India.*

[b]*School of Basic Sciences, Indian Institute of Technology Bhubaneswar, Bhubaneswar 751013, Odisha, India.*

[c]*Department of Life Science, National Institute of Technology, Rourkela 769008, Odisha, India.*

[d]*Fribourg Center for Nanomaterials, Department of Chemistry, University of Fribourg, CH-1700 Fribourg, Switzerland.*

[e]*Department of Inorganic and Physical Chemistry, Indian Institute of Science, Bangalore 560012, India.*

Abstract

4–(p–X–phenyl) thiosemicarbazone of napthaldehyde {where, X = Cl (HL^1) and X = Br (HL^2)}, thiosemicarbazone of quinoline–2–carbaldehyde (HL^3) and 4–(p–fluorophenyl) thiosemicarbazone of salicylaldehyde (H_2L^4) and their copper(I), {$[Cu(L^1)(PPh_3)_2Br]\cdot CH_3CN$ (**1**) and $[Cu(L^2)(PPh_3)_2Cl]\cdot DMSO$ (**2**)} and copper(II), {$[(Cu_2L^3{}_2Cl)_2(\mu–Cl)_2]\cdot 2H_2O$ (**3**) and $[Cu(L^4)(Py)]$ (**4**)} complexes are reported. The synthesized ligands and their copper complexes were successfully characterized by elemental analysis, cyclic voltammetry, NMR, ESI–MS, IR and UV–Vis spectroscopy. Molecular structures of all the Cu(I) and Cu(II) complexes have been determined by X–ray crystallography. All the complexes (**1**–**4**) were tested for their ability to exhibit DNA binding and cleavage activity. The complexes effectively interact with CT–DNA possibly by groove binding mode, with binding constants ranging from $10^4 - 10^5$ M^{-1}. Among the complexes, **3** show highest chemical (60%) as well as photo-induced (80%) DNA cleavage activity against pUC19 DNA. Finally, the *in vitro* antiproliferative activity of all the complexes was assayed against the HeLa cell line. Some of the complexes proved to be as active as the clinical referred drugs, and the greater potency of **3** may be correlated with its aqueous solubility and the presence of quinonoidal group in the thiosemicarbazone ligand coordinated to the metal.

Introduction

Cisplatin (*cis*−diamminedichloroplatinum(II)) is a well-known metal based drug for cancer, despite of its wide application as a chemotherapeutic agent, cisplatin exhibits severe side effects, such as nausea, kidney and liver failure, typical of heavy metal toxicity.[1–5] Therefore endeavors are constantly made to replace it with suitable alternatives; hence various transition metal complexes have been synthesized and tried for their anticancer properties.

Metal complexes which efficiently bind and cleave DNA under physiological conditions are considered as potential to be used as therapeutic agents for medicinal applications and for genomic research.[6–9] Depending on the exact nature of the metal and ligand, the complexes can bind with nucleic acid covalently or non-covalently.[10,11] Non-covalent interactions between transition-metal complexes and DNA can occur by intercalation, groove binding, or external electrostatic binding. Therefore, the study on the interaction of the transition metal complexes with DNA is of great significance for the design of new drugs and their application.

Among the transition metals, the coordination chemistry of the copper attracts increasing interest because of the use of many copper complexes as models for biological functions, such as amine oxidases,[12] catechol oxidase,[13] nitrite reductase,[14] superoxide dismutase[15] and tyrosinase.[16] Copper complexes have been extensively utilized in metal ion mediated DNA cleavage through the hydrogen ion abstraction by activated oxygen species.[17] In the recent years, a large number of biocompatible Cu(II) complexes, have been investigated for their anticancer property.[18]

Additionally, thiosemicarbazones (TSCs) are a class of Schiff bases which are considered as one of the most important scaffolds and are embedded in many biologically active compounds.[19] Brockman et al. first reported that 2-formylpyridine TSC possesses antileukemic activity in mice.[20] Following this report, various aliphatic, aromatic, and heteroaromatic carbaldehyde TSCs were synthesized and evaluated for their antitumor activity against a wide spectrum of transplanted murine neoplasms.[21–25] The lists of TSC derivatives have been found to exhibit intense anticancer activities are shown in Chart 1.[18b,26] Again, the transition metal complexes with TSCs as ligands have raised interest amongst many researchers, and they continue to be the subject of many studies, especially as anticancer chemotherapeutic[27–29] and as DNA–binding and cleaving agents.[18b,30] TSC complexes have also demonstrated significant activity as antitumor, antiviral, antimicrobial, anti–amoebic and anti–inflammatory agents[31–33]. Many Cu complexes of TSCs have demonstrated efficient antitumor potential.[18b,18c,26a,26b,34–38] Although the chemistry of Cu(II) TSC complexes is well developed,[30g,39–41] relatively less information is available for Cu(I) complexes,[42–46] particularly related to their pharmacological properties.

Again, while many TSC complexes exhibit good biological activities, their water solubility is still unsatisfactory, which may restrict their application. Hence, it seemed of interest to synthesize some new water–soluble transition metal complexes of TSCs which may have significant pharmacological effects.

Considering these facts and as a continuation of our ongoing research on the study of pharmacological properties[47] of transition metal complexes, in this report, two new Cu(I) complexes {$[Cu(L^1)(PPh_3)_2Br]\cdot CH_3CN$ (**1**) and $[Cu(L^2)(PPh_3)_2Cl]\cdot DMSO$ (**2**)}, a novel tetranuclear copper(II) complex $[(Cu_2L^3{}_2Cl)_2(\mu\text{–}Cl)_2]\cdot 2H_2O$ (**3**) and a new Cu(II)

monomeric complex [Cu(L^4)(Py)] (**4**) were synthesized and fully characterized. The interaction of these complexes with calf−thymus DNA (CT–DNA) utilizing UV–Vis absorption titration, competitive DNA binding fluorescence experiments, circular dichroism and thermal denaturation studies were studied. Their chemical as well as photo-induced cleavage activity with pUC19 supercoiled plasmid DNA were investigated. Furthermore, the cytotoxicity of the complexes against the HeLa cell line was surveyed by the MTT assay.

Experimental

Materials and methods

All chemicals were purchased from commercial sources and used without further purification. Reagent grade solvents were dried and distilled prior to use. The thiosemicabazides were prepared from distilled substituted aniline by a known method reported ear1ier.[48] The ligands 4–(p–X–phenyl) thiosemicarbazone of napthaldehyde {where X = Cl (HL^1) and X = Br (HL^2)}, thiosemicarbazone of quinoline–2–carbaldehyde, (HL^3) and 4–(p–fluorophenyl) thiosemicarbazone of salicylaldehyde (H_2L^4) were prepared by reported methods.[47c,49] MTT (3–[4,5–dimethylthiazol–2–yl]–2,5–diphenyl tetrazolium) and DAPI (4′,6–diamidino–2–phenylindole dihydrochloride) were purchased from Sigma Aldrich (USA). Minimal essential medium (MEM) was purchased from Gibco, India. The supercoiled (SC) pUC19 DNA was purified from *E. coli* cells with the aid of GeneJET Plasmid Isolation Kit (Thermo Scientific, USA). Calf thymus (CT) DNA was purchased from SRL (India) (biochemistry grade). Elemental analyses were performed on a Vario ELcube CHNS Elemental analyzer. IR spectra were recorded on a Perkin–Elmer Spectrum RXI spectrometer. ^{1}H, ^{13}C and ^{31}P NMR spectra were recorded with a Bruker Ultrashield 400 MHz spectrometer using $SiMe_4$ as an internal standard. Electronic spectra were recorded on a Lamda25, PerkinElmer spectrophotometer. Mass spectra were obtained on a SQ–300 MS instrument operating in ESI mode. Electrochemical data were collected using PAR electrochemical analyzer and a PC-controlled potentiostat/galvanostat (PAR 273A) at 298 K in a dry nitrogen atmosphere. Cyclic voltammetry experiments were carried out with Pt working and auxiliary electrodes and Ag/AgCl as reference electrode and TEAP as supporting electrolyte. Commercially available TEAP (tetra ethyl ammonium perchlorate) was properly dried and used as a supporting electrolyte for recording cyclic voltammograms of the complexes.

Synthesis of complexes {$[Cu(L^1)(PPh_3)_2Br]\cdot CH_3CN$ (1) and $[Cu(L^2)(PPh_3)_2Cl]\cdot DMSO$ (2)}

Cu(I)X (X = Br/Cl) (1.0 mmol) was added to a solution of the ligand $HL^{1–2}$ (1.0 mmol) in 20 mL of CH_3CN, the contents were refluxed for 1 h, followed by the addition of PPh_3 (1.0 mmol) and continued refluxing for another 1 h. The resulting yellow solution was filtered and slow evaporation of the filtrate over 4–5 days produced yellow crystalline product. Crystals suitable for X-ray analysis were isolated for complex **1**. X–ray quality crystals of complex **2** were obtained by recrystallizing in DMSO.

$[Cu(L^1)(PPh_3)_2Br]\cdot CH_3CN$ (1): Yield: 67%. Anal. calc. for $C_{56}H_{47}BrClCuN_4P_2S$: C, 64.12; H, 4.52; N, 5.34. Found: C, 64.13; H, 4.54; N, 5.38. Main IR peaks (KBr, cm^{-1}): 3285m ν(N(1)–H), 3049m ν(N(2)–H), 2901m ν(C(8)–H), 1632s ν(C=C), 1547s ν(–C(8)=N(3)), 1096s ν(P–C_{Ph}), 770s ν(C(7)=S). ^{1}H NMR (DMSO–d_6, 400 MHz) δ: 12.03 (s, 1H, –C(7)–N(1)H), 10.25 (s, 1H, –C(7)–N(2)H), 9.094 (s, 1H, –N(3)=C(8)H), 8.42–7.27 (m, 26H, Ph + PPh_3). ^{13}C NMR (DMSO–d_6, 100 MHz) δ: 175.39 (C(7), C–S), 138.6 (C(8), N=CH), 136.72, 136.32, 135.87, 135.23, 134.85, 134.43, 133.81, 133.12, 132.83, 132.25, 131.91, 131.33, 130.78, 130.26, 130.02, 129.83 (16C, C_6H_6), 128.96, 128.47, 127.80 (PPh_3). ^{31}P NMR

(DMSO–d_6, 162 MHz) δ: 46.26 and 44.79 (2s, 2PPh_3). ESI MS (CH_3OH): *m/z* 1047.74 (100%, $[M - H]^+$); *m/z* 1071.95 (30%, $[M + Na]^+$); *m/z* 1087.69 (65%, $[M + K]^+$).

$[Cu(L^2)(PPh_3)_2Cl]\cdot DMSO$ (2): Yield: 67%. Anal. calc. for $C_{56}H_{50}BrClCuN_3OP_2S_2$: C, 61.93; H, 4.64; N, 3.87. Found: C, 61.90; H, 4.67; N, 3.88. Main IR peaks (KBr, cm^{-1}): 3284m ν(N(1)–H), 3047m ν(N(2)–H), 2908m *ν*(C(8)–H), 1627s *ν*(C=C), 1551s *ν*(–C(8)=N(3)), 1090s ν(P–C_{Ph}), 768s ν(C(7)=S). ^{1}H NMR (DMSO–d_6, 400 MHz) δ: 12.47 (s, 1H, –C(7)–N(1)H), 10.29 (s, 1H, –C(7)–N(2)H), 9.09 (s, 1H, –N(3)=C(8)H), 8.07–7.25 (m, 26H, Ph + PPh_3), 2.53 (s, 6H, DMSO). ^{13}C NMR (DMSO–d_6,100 MHz) δ:178.18 (C(7), C–S), 140.51 (C(8), N=CH), 137.82, 137.12, 136.87, 135.73, 134.95, 134.41, 133.85, 133.19, 132.79, 132.41, 131.86, 131.23, 130.96, 130.26, 130.12, 129.92 (16C, C_6H_6), 129.12, 128.87, 128.17 (PPh_3). ^{31}P NMR (DMSO–d_6, 162 MHz) δ: 46.85 and 44.72 (2s, 2PPh_3). ESI MS (CH_3OH): *m/z* 1086.70 (12%, $[M + H]^+$); *m/z* 1051.92 (20%, [M – Cl]).

Synthesis of complex $[(Cu_2L^3{}_2Cl)_2(\mu\text{–}Cl)_2]\cdot 2H_2O$ (3)

$CuCl_2\cdot 2H_2O$ (1.0 mmol) was added to a solution of Ligand, HL^3 (1.0 mmol) in 20 mL of hot methanol and the mixture was refluxed for 2 h. The resulting dark green solution was filtered and slow evaporation of the filtrate over 4–5 days produced deep green crystals suitable for X–ray analysis.

$[(Cu_2L^3{}_2Cl)_2(\mu\text{–}Cl)_2]\cdot 2H_2O$: Yield: 58%. Anal. calc. for $C_{44}H_{40}Cl_4Cu_4N_{16}S_4O_2$: C, 39.17; H, 2.99; N, 16.61. Found: C, 39.19; H, 2.97; N, 16.63. Main IR peaks (KBr, cm^{-1}): 3228m ν(–N(1)–H_2), 3047m *ν*(C(2)–H), 1635s *ν*(C=C), 1557s, *ν*(–C(2)=N(3)) 752s ν(C(1)–S). ESI MS (CH_3OH): *m/z* 1318.80 (68%, $[(M - 2H_2O) + 5H]^+$); *m/z* 1352.55 (100% $[(M + 3H]^+$).

Synthesis of complex $[Cu(L^4)(Py)]$ (4)

$CuCl_2\cdot 2H_2O$ (1.0 mmol) was added to a solution of H_2L^4 (1.0 mmol) in 20 ml of hot methanol followed by the addition of pyridine (1.0 mmol). The mixture was refluxed for 3 h and a clear bluish green solution was obtained, which was filtered and slow evaporation of the filtrate over 3–4 days produced bluish green crystals suitable for X–ray analysis.

$[Cu(L^4)(Py)]$: Yield: 67%. Anal. calc. for $C_{19}H_{15}CuFN_4OS$: C, 53.08; H, 3.52; N, 13.03. Found: C, 53.11; H, 3.56; N, 13.07. Main IR peaks (KBr, cm^{-1}): 3224s ν(N(1)–H), 2356m *ν*(C(8)–H), 1602s ν(C=C), 1531s ν(–C(8)=N(3)), 748s ν(C(7)–S(1)). ESI MS (CH_3OH): *m/z* 430.07 (100%, $[M]^+$); *m/z* 431.72 (50%, $[M + H]^+$); *m/z* 351.14 (46%, $[M - Py]^+$).

Crystallography

Single crystals of complexes were mounted on Stoe IPDS 2 diffractometer equipped with an Oxford Cryosystem open flow cryostat. (**1** & **2**) & Bruker Smart Apex CCD diffractometer (**3** & **4**), equipped with a graphite monochromator and a Mo Kα radiator (λ) 0.71073 Å. Crystallographic data and details of refinement of **1**–**4** are given in Table 1. The unit cell dimensions and intensity data were measured at 200(2) K for **1** & **2**, 273(2) K for **3** & 296(2) for **4**. Absorption correction was partially integrated in the data reduction procedure for crystals of **1** & **2**.[50] The intensity data were corrected for Lorentz, polarization and absorption effects. Absorption corrections were applied using SADABS[51] and the structures were solved by direct methods using the program SHELXS−97[52] and refined using least squares with the SHELXL−97[52] software program.

Hydrogens were either found or placed in calculated positions and isotropically refined using a riding model. The non-hydrogen atoms were refined anisotropically.

DNA binding experiments

(a) Absorption spectral studies

The DNA binding experiments were performed with Perkin−Elmer Lamda35 spectrophotometer as described previously.[47e] Briefly, the absorption titration experiments were performed by varying the concentration of CT−DNA from 0 to 70 μM and keeping the metal complex concentration constant at 25 μM in 10 mM Tris–HCl buffer (pH 8.0) containing 1% DMF. The binding constant K_b was computed from the data obtained using the following equation[47e]

$$\frac{[DNA]}{\varepsilon_a - \varepsilon_f} = \frac{[DNA]}{\varepsilon_b - \varepsilon_f} + \frac{1}{K_b(\varepsilon_b - \varepsilon_f)}; \qquad \text{Eq. 1}$$

where [DNA] is the concentration of DNA base pairs, ε_a, ε_f and ε_b correspond to apparent extinction co−efficient for the complex *i.e.* Abs/[complex] in presence of DNA, in absence of DNA and to fully bound DNA respectively. A plot of $[DNA]/(\varepsilon_a - \varepsilon_f)$ *vs* [DNA] gave a slope and the intercept equal to $1/(\varepsilon_b - \varepsilon_f)$ and $1/K_b(\varepsilon_b - \varepsilon_f)$, respectively. The binding constant K_b was calculated from the ratio of the slope to the intercept. Ligand interaction with CT−DNA were also studied by titrating a fixed concentration of ligand (25 μM) with variable CT−DNA concentration ranging from 0−350 μM in 10 mM Tris–HCl buffer (pH 8.0) containing 1% DMF.

(b) Competitive DNA binding fluorescence measurements

The apparent binding constant (K_{app}) for the complexes were determined by fluorescence measurements using ethidium bromide (2 μM) (EB) bound CT−DNA (50 μM) solution in 10 mM Tris–HCl buffer (pH 8.0) containing 1% DMF with the aid of Fluoromax 4P spectrofluorimeter (Horiba Jobin Mayer, USA). The fluorescence intensities of EB at 597 nm (excitation 510 nm) with an increasing amount of the complex concentration (0−60 μM) was measured. In the presence of DNA, EB showed enhanced emission intensity due to intercalative binding with DNA. A competitive binding of metal complexes with CT−DNA leads to the decrease in the emission intensity due to emission quenching or the displacement of bound EB to CT−DNA by the complexes. The quenching constant was calculated by using the following Stern−Volmer equation[53]

$$\frac{F_0}{F} = 1 + K_{SV}[Q] \qquad \text{Eq. 2}$$

where F_0 and F are the emission intensity of EB bound CT–DNA in absence and in presence of the quencher (complexes) concentration [Q] respectively, gave the Stern−Volmer quenching constant (K_{SV}).The apparent binding constant (K_{app}) was calculated from the following equation.

$$K_{EB} \times [EB] = K_{app} \times [complex]_{50} \qquad \text{Eq. 3}$$

where K_{app} is the apparent binding constant of the complex, $[complex]_{50}$ is the concentration of the complex at 50% quenching of the emission intensity of EB bound CT–DNA, K_{EB} is the binding constant of EB ($K_{EB} = 1.0 \times 10^7\ M^{-1}$) and [EB] is the concentration of ethidium bromide (2 μM).[53]

(c) Thermal melting studies

Thermal melting studies of CT−DNA (100 μM) in the absence and presence of complexes (50 μM) were carried out by monitoring the absorbance at 260 nm in the temperature range of 30−90°C with a ramp rate of 0.5°C/min in 10 mM Tris−HCl buffer (pH 8.0) containing 1% DMF. The experiments were carried out using a Chirascan CD spectropolarimeter (Applied Photophysics, UK) in absorbance mode equipped with temperature controller. The melting temperature (T_m) was determined from the derivative plot (dA_{260}/dT *vs* T) of the melting profile.[47e]

(d) Circular dichroism studies

The Circular Dichroism (CD) spectroscopic studies were performed using Chirascan CD spectropolarimeter (Applied Photophysics, UK) at 25°C. CD spectra of CT–DNA (50 μM) in absence and presence of complexes (10 μM) were obtained in the wavelength range of 240–400 nm in 10 mM Tris–HCl buffer (pH 8.0) containing 1% DMF, using quartz cell with 10 mm path length.[47e]

DNA cleavage experiments

DNA cleavage was carried out as previously reported.[47e] The chemical−induced and photo−induced DNA cleavage experiments were done with 300 ng supercoiled (SC) pUC19 DNA in 50 mM Tris–HCl buffer (pH 8.0) containing 1% DMF.

(a) Chemical−induced DNA cleavage

In order to study the chemical nuclease activity of the complexes, reactions were performed in the dark using hydrogen peroxide (0.5 mM) as the oxidising agent in absence and presence of complexes (1–300 μM). The solutions were incubated at 37°C for 1 h and analysed for DNA cleaved products by agarose gel electrophoresis.

(b) Photo-induced DNA cleavage

The photo−induced DNA cleavage activity was performed as described previously.[47e] Briefly, the photo−induced DNA cleavage experiments were carried out using UVA source at 350 nm (Luzchem Photoreactor Model LZC–1, Ontario, Canada) fitted with 14 UVA tubes (84 W) for 1 h, on supercoiled (SC) pUC19 DNA (300 ng) with complexes (1–300 μM) in 50 mM Tris−HCl buffer (pH 8.0) containing 1% DMF. DNA cleavage was indicated by the decrease in the supercoiled pUC19 DNA (Form I) and subsequent formation of nicked circular DNA (Form II) and linear DNA (Form III). The percentage of net DNA cleavage was calculated by the following equation:

$$\text{Net DNA cleavage \%} = \frac{\text{Form IIs}+2\times\text{Form IIIs}}{\text{Form Is}+\text{Form IIs}+2\times\text{Form IIIs}} - \frac{\text{Form IIc}+2\times\text{Form IIIc}}{\text{Form Ic}+\text{Form IIc}+2\times\text{Form IIIc}} \qquad \text{Eq. 4}$$

The subscripts "s" and "c" refers to the sample and control respectively.[54] Appropriate DNA controls were taken to calculate the net DNA cleavage percent. The observed error in measuring the band intensities ranged between 3% – 6%.

For mechanistic investigations of both hydrolytic and photolytic DNA cleavage, experiments were carried out with singlet oxygen quenchers such as sodium azide (NaN_3) and L−histidine, while for hydroxyl radical scavengers potassium iodide (KI) and D−mannitol were used. Each of the additives was used at a concentration of 0.5 mM.

Anticancer Activity

(a) Cell Culture

Human cervical cells HeLa were obtained from National Centre of Cell Science (NCCS), Pune, India and were maintained in minimal essential medium supplemented with 10% fetal bovine serum, penicillin-streptomycin solution and incubated at 37°C in 5% CO_2 and 95% humidified incubator. The complexes were dissolved in DMSO at a concentration of 100 mM as stock solution, and diluted in culture medium at concentrations of 12.5, 25.0, 50.0 and 100.0 μM as working solution. To avoid DMSO toxicity, the concentration of DMSO was less than 0.1% (v/v) in all experiments.

(b) Cytotoxic Assay

HeLa cells were harvested from maintenance cultures in logarithmic phase, after counting in a hemocytometer using trypan blue solution. The cell concentration was adjusted to $5x10^4$ cells/ml and the cells were plated in 96 well flat bottom culture plates and incubated for 72 h with various concentrations of the test compounds. The effect of the drugs on the cancer cell viability was studied using MTT dye reduction assay by measuring the optical density at 595 nm using micro−plate reader spectrophotometer (Perkin−Elmer 2030).[55]

(c) Nuclear Staining

Nuclear staining using DAPI stain was performed according to the method previously described.[56] Briefly, HeLa cells either treated or untreated with test compounds were smeared on a clean glass slide, cells were fixed with 3.7% formaldehyde for 15 minutes, permeabilized with 0.1% Triton X−100 and stained with 1 μg/ml DAPI for 5 min at 37°C. The cells were then washed with PBS and examined by fluorescence microscopy (Olympus IX 71) to ascertain any condensation or fragmentation of the nuclei indicating cells undergoing apoptosis.

Results and discussion

Synthesis

Reaction of Cu(I)X (X = Cl, Br) with 4–(p–X–phenyl) thiosemicarbazone of napthaldehyde {X = Cl (HL^1); X = Br (HL^2)} in the molar ratio of 1:1 in CH_3CN formed an insoluble product of stoichiometry $[CuX(HL^{1-2})]$ which after addition of two moles of PPh_3 yielded light yellow colored monomeric complexes $[CuX(HL^{1-2})(PPh_3)_2]\cdot$Solvent (X = Br, **1**; Cl, **2**). Reaction of copper(II) chloride with quinoline–2–carbaldehyde thiosemicarbazone (HL^3) in the molar ratio of 1:1 in CH_3OH yielded dark green colored tertrameric complex $[(Cu_2L^3{}_2Cl)_2(\mu\text{–}Cl)_2]\cdot 2H_2O$ (**3**) whereas with 4–(p–F–phenyl) thiosemicarbazone of salicylaldehyde (H_2L^4) in presence of pyridine as coligand yielded dark green monomeric complex $[Cu(L^4)(Py)]$ (**4**). The electrospray mass spectra (ESI MS) and NMR spectra were consistent with the X–ray structures. The purity of these compounds was further confirmed by elemental analyses. The synthetic methods of all the complexes are illustrated in Scheme 1. All complexes were soluble in MeOH, MeCN, DMF and DMSO. Complex **3** was completely and other three complexes (**1**, 38%; **2**, 35% and **4**, 45%, H_2O–DMSO solution) were partially soluble in H_2O. All the complexes were stable in both solid and solution phases. The solution phase stability of the complexes was confirmed by electronic absorption, NMR and ESI–MS spectral studies. The representative spectra are given in ESI Fig. S1, Fig. S2 and Fig S3.

Structure

The observed elemental (C, H, N) analytical data of all the complexes **(1**–**4)** are in consistent with their composition. It appears from the formulation of **1** & **2** that the TSC is serving as a monodentate ligand where as in **3** & **4** it is serving as a tridentate ligand. In order to authenticate the coordination mode of the TSC in the complexes, the structures has been determined by X–ray crystallography.

Description of X-ray structures of $[Cu(L^1)(PPh_3)_2Br]\cdot CH_3CN$ (1) and $[Cu(L^2)(PPh_3)_2Cl]\cdot$DMSO (2):

The molecular structure and the atom numbering scheme for the complexes $[Cu(L^1)(PPh_3)_2Br]\cdot CH_3CN$ (**1**) and $[Cu(L^2)(PPh_3)_2Cl]\cdot$DMSO (**2**) are shown in Fig. 1 and Fig. 2 respectively; the relevant bond distances and angles are collected in Table 2. Compounds **1** and **2** contain CH_3CN and DMSO as a solvent of crystallization respectively. The coordination geometry around the Cu(I) atom in **1** and **2** reveals a distorted tetrahedral environment with an SXP_2 [X = Br (**1**) and Cl (**2**)] coordination sphere as the bond angles around the copper atom vary from ca. 100–124° in **1** and **2** with P−Cu−P being the largest angle.[49,57] The ligand HL^{1-2} acts as a monodentate ligand coordinating through the S atom. The other positions of the tetrahedron are occupied by one halogen atom and two triphenylphosphine ligands. In the compound, the Cu−S bond lengths are 2.401(7) Å for **1** and 2.387(1) Å for **2**, while the Cu-halogen bond distances lie in ranges 2.374(1)–2.517(4) Å as usually found for tetrahedrally coordinated copper(I) and S atom donors.[44,49] The Cu−P distances [2.276(6), 2.290(7) Å for **1**, 2.274(1), 2.295(1) Å for **2**] are comparable to those found in similar complexes. [44,49]

Description of X-ray structure of $[(Cu_2L^3{}_2\,Cl)_2(\mu\text{–}Cl)_2]\cdot 2H_2O$ (3):

The structure of the tetranuclear Cu(II) complex $[(Cu_2L^3{}_2\,Cl)_2(\mu\text{–}Cl)_2].2H_2O$ is illustrated in Fig. 3 and selected bond parameters are collected in Table 3. Compounds **3** contain two H_2O molecules as solvent of crystallization. The structure contains four units comprising of two identical Cu(1)LCl outer units and two identical Cu(2)LCl inner units. In other words, the tetranuclear Cu(II) species is formed by the dimerisation of two binuclear $Cu_2L_2Cl_2$ units bridged by two reciprocal coordinated chlorine atoms of the individual $Cu_2L_2Cl_2$ unit. Each copper atom in the outer unit is coordinated by a quinoline nitrogen, azomethine nitrogen and thiolate sulfur of the thiosemicarbazone moiety and a chlorine group. The $Cu\text{–}N_{quinoline}$ bonds are ~ 0.131 Å farther away than $Cu\text{–}N_{imine}$ bonds, denoting the strength of the azomethine nitrogen coordination. The length of the other metal coordinated bonds (Cu−S and Cu−Cl) is usual like similar systems reported earlier.[58,59] The bond angles also are in conformity with a distorted square pyramidal structure around the copper centers. Each copper atom in the inner subunit is pentacoordinate with the bonds Cu(2)–S(2), Cu(2)–Cl(2), Cu(2)–N(8), Cu(2)–N(7) and Cu(2)–Cl(2)# adapting a distorted square pyramidal geometry with bridging Cl(2)# of the other inner moiety at the apical site. The quinoline nitrogen N(8), the imino nitrogen N(7), and the thiolate sulfur S(2) atom, together with Cl(2), constitute the basal plane. The bond lengths in the basal plane agree with those found in copper(II) complexes containing thiosemicarbazones which act as uninegative tridentate ligands.[58,59] The bond lengths and bond angles reveal a distorted square pyramidal geometry around Cu(2).

Description of X-ray structure of $[Cu(L^4)(Py)]$ (4):

The atom numbering scheme for the complex **4** is given in Fig. 4 with the relevant bond distances and angles collected in Table 3. The structure shows that the thiosemicarbazone ligand (L^{2-}) is coordinated to copper in the expected tridentate fashion (Scheme 1), forming a six− and a five−membered chelate ring with O(1)–Cu(1)–N(3) and S(1)–Cu(1)–N(3) bite angles of 94.04(7)º and 85.92(5)° respectively. The co−ligand pyridine is coordinated to the metal center, and is trans to the nitrogen atom N(3). The rather large Cu(1)−N(4) distance is 2.013(1) Å revealed that the pyridine moiety is weakly coordinated to the Cu−center.[60] Copper is thus nested in a NOSN core, which is slightly distorted from an ideal square-planar geometry, as reflected in the bond parameters around the metal center. The Cu–N(3), Cu–O(1), Cu–N(4) (co-ligand) and Cu–S(1) distances are normal, as observed in other structurally characterized complexes of Cu containing these bonds.[60,61]

Spectral Characteristics

The IR spectra of **1** & **2** showed the presence of ν(N–H) bands in the ranges 3284–3285 cm^{-1} for –N(1)–H and 3047–3049 cm^{-1} for –N(2)–H stretching, which suggests that the thiosemicarbazone ligand are coordinated to the Cu(I) centre in the neutral form. In all the complexes (**1**–**4**) ν(C=N) and ν(C=C) vibrational modes appeared in the range 1635–1531 cm^{-1}, while the thioamide bands ν(C–S (**1** & **2**) & C=S (**3** & **4**)) appeared in the range 770–748 cm^{-1} (compared to free ligands, 854–785 cm^{-1}).[47c,] The characteristic $\nu(P\text{–}C_{Ph})$ bands at 1096–1090 cm^{-1} indicate the presence of Ph_3P in **1** & **2**.

The electronic spectra of all the complexes (Table 4) were recorded in methanol solutions. In the spectra of **1**–**4** three strong absorptions are observed in the wavelength range 448–220 nm. The lower energy absorptions at around 448–349 nm are ascribable to metal to ligand (**1** & **2**) the ligand to metal (**3** & **4**) charge transfer transitions whereas the higher energy absorptions are likely to be due to ligand centered transitions.[46,47c] Weak absorptions in the range 676−668 nm are also observed for **3** & **4** (Cu(II) complexes), which are assigned to d−d transitions.[62]

The NMR spectra (^{1}H, ^{13}C and ^{31}P) of **1** & **2** were recorded using DMSO–d_6. The ^{1}H NMR spectrum exhibits three singlets in the range 12.47–9.09 ppm due to NH (–C(7)–N(1)H), NH (–C(7)–N(2)H) and CH (–N(3)=C(8)H) groups respectively. Signals for aromatic protons found as multiplets in 8.42–7.25 ppm range.[47c] The ^{13}C NMR spectra of the complexes (**1** & **2**) showed a sharp singlet appearing at 178.18–175.39 ppm due to C–S carbon. The peak for the azomethine (–CH=N) carbon exhibited a peak in the region 140.51–138.6 ppm. The peaks observed in the 137.82–129.83 ppm region have been assigned to aromatic carbons. The PPh_3 peaks are assigned in the range 129.12–127.80 ppm.[63] ^{31}P NMR spectra were recorded in order to confirm the presence of triphenyl phosphine group. The two signals appeared at 46.85–44.72 ppm and indicated that the two triphenyl phosphine ligands were *cis* to each other in these complexes.[63] The detailed NMR data has been included in the experimental section.

ESI mass spectra of **1**−**4** have been recorded in methanol solution. Mass spectral analysis for **1** and **2** shows peaks at m/z 1047.34 $[(M + H)^+]$ and 1086.70 $[(M + H)^+]$ respectively, whereas **3** shows the molecular ion peak $[(M + 3H)^+]$ at m/z 1352.55. ESI–MS peak for **4** shows the characteristic molecular ion peak (M^+) at m/z 430.07. ESI Fig. S4 depicts a representative ESI mass spectrum of **4**.

Electrochemical properties

The electrochemical properties of **1**–**4** were examined in CH_3CN solution (0.1 M TEAP) by cyclic voltammetry using a platinum working electrode, platinum auxiliary electrode and an Ag/AgCl reference electrode. The potential data are listed in Table 5. Figs. 5, 6 and 7 depicts the representative voltammogram of **1** {Cu(I)}, **3** {Cu(II)} and **4** {Cu(II)} respectively. The voltammograms of all four complexes include both oxidation and reduction processes. The voltammogram pattern is similar for **1** & **2**, which includes a quasireversible (Fig. 5) process at $E_{1/2}$ value 0.37 to 0.40 V corresponding to Cu(I)/Cu(II) redox couple.[46] Whereas in the cathodic region (ESI Fig. S5) Cu(I) is reduced to Cu(0) showing an irreversible single electron wave at E_{pc} values within the potential window –0.70 to –0.72 V.[64]

In the voltammogram of tetrameric Cu(II) complex (**3**), there are three quasireversible/reversible (Fig. 6) processes at $E^{c/a}_{1/2}$ values –0.62, 0.10 and 0.36 V corresponding to Cu(II)/Cu(I) redox couples[65] of four different Cu(II) centers, whereas for the monomeric Cu(II) complex (**4**) a quasireversible (Fig. 7) process for the above couple appears at $E^{c}_{1/2}$ value –0.52 V.

For all four complexes (**1**−**4**) an oxidation peak (ESI Fig. S6) in the range 0.87 to 0.91 V[66] and two reduction peaks (ESI Fig. S5) in the range –1.37 to –1.45 and –1.61 to –1.65 V[31,47c] belongs to ligand centered processes respectively. A representative oxidative votammogram of a free ligand HL^3 is given in ESI Fig. S7.

DNA binding studies

(a) Absorption spectroscopic studies

DNA is often a vital target to mediate apoptosis or necrosis to a cell. Therefore the binding affinity of the complexes to CT–DNA was studied using different spectral methods. UV–Vis titration experiments were carried out to determine the binding constant (K_b) of the complexes to CT–DNA (Fig. 8 and Table 6). The complexes **1**–**4** shows absorption bands in the region 448–349 nm which is attributed to metal to ligand (**1** & **2**) and ligand to metal (**3** & **4**) charge transfer transition whereas the absorption bands at higher energy is due to intra-ligand transition. Binding of complexes to DNA either leads to hypochromism or hyperchromism which provides a measure of strength for intercalative or groove binding respectively.[67]

In order to quantify the binding affinity of the interaction between CT–DNA and each of **1**–**4**, the binding constant (K_b) was calculated using Eq. 1 (*Experimental Section*). The binding constant (K_b) of the complexes were in the range of 1.30×10^4 to 9.60×10^5 M^{-1}. Copper(I) complexes, **1** and **2** exhibited higher binding affinity than copper(II) complexes **3** and **4**. The binding propensities of ligands to CT–DNA were also estimated. All the ligands showed lesser DNA binding affinity than their respective complexes, yielding K_b values in the order of 10^3 M^{-1} (ESI Fig. S8 and Table S1).

(b) Competitive DNA binding fluorescence studies

Ethidium dibromide (EB) is a standard intercalating agent and exhibits fluorescence upon binding to DNA. The relative binding of the complexes **1**–**4** to CT–DNA was also investigated by monitoring the quenching of the fluorescence emission from EB bound CT–DNA, on successive addition of the complexes. EB is non emissive in 10 mM Tris–HCl buffer (pH 8.0) containing 1% DMF due to fluorescence quenching of free EB by solvent molecules. While in the presence of DNA, EB shows enhanced emission intensity due to intercalative binding.[68] On addition of the copper complexes to EB bound CT–DNA, the emission intensity at 597 nm was quenched by ~ 14% and ~ 13% for copper(I) complexes **1** and **2** respectively, whereas copper(II) complexes **3** and **4** exhibited a decrease of ~ 82% and ~ 10% respectively (Fig. 9). The quenching of emission intensity of ethidium bromide upon addition of **1**–**4** showed that the complexes probably compete with EB for the binding with DNA. Copper(I) complexes **1** and **2** exhibited a Ksv value of 3.06×10^3 and 2.22×10^3 M^{-1} as calculated from Eq. 2 and the K_{app} value of 6.87×10^5 and 6.70×10^5 M^{-1} as calculated from Eq. 3 respectively (Table 6). Similarly for copper(II) complexes, **3** exhibited the highest decrease in the emission intensity of EB which is well reflected in its Ksv and K_{app} values of 5.36×10^4 and 7.34×10^5 M^{-1} respectively. Complex **4** showed the least decrease in the emission intensity of EB which is in coherence with its lower Ksv and K_{app} value of 1.32×10^3 and 5.79×10^5 M^{-1} respectively (Table 6). The higher Ksv and K_{app} value of **3** than the other complexes may be attributed to its higher solubility in aqueous medium and the presence of quinonoidal group in the thiosemicarbazone ligand coordinated to the metal.

The K_{app} of the complexes were ~10^2 order lesser than the classical intercalator EB (i.e. 1.00×10^7 M^{-1}), which suggest that the interaction between the complexes and CT–DNA were possibly groove binding in nature. The K_{app} values gave a similar trend of competitive DNA binding propensities of the complexes as obtained from UV–Vis absorption spectral studies.

Control competitive DNA binding experiments with ligands showed that ligands have lesser Ksv and K_{app} values than their corresponding complexes (ESI Fig. S9 and Table S1).

(c) Thermal melting studies

In order to have an insight into the nature of interaction and the conformational changes brought about by the complexes on interaction with CT–DNA, thermal denaturation experiments were performed.[69] The melting temperature of CT–DNA (T_m) in absence of any complexes was ~65.7 ^oC (Fig. 10). In the presence of the copper complexes the DNA melting temperature (T_m) showed a slight increase from ~1.05^oC to 1.83^oC (Table 6). Among all the complexes, **3** showed the highest shift of the DNA melting temperature (ΔT_m) of + 1.83^oC which may be accounted for its better interaction with CT–DNA as evidenced from UV–Vis absorption and competitive DNA binding studies. The lower ΔT_m values suggest that the complexes interact with CT–DNA primarily through groove binding mode rather than an intercalative mode of binding to DNA which generally results in higher positive shift in the T_m of CT–DNA.[69,70]

(d) Circular dichroism studies

Circular dichroism was used to investigate the conformational changes in CT–DNA due to the interaction with the complexes. CT–DNA shows two conserved bands in the UV region, a positive band at 275 nm due to base stacking interaction and a negative band at 245 nm due right handed helicity.[71] The interaction of **1**, **2** and **4** showed marginal changes in the CD spectra of CT–DNA, whereas the interaction of **3** with CT–DNA induced a decrease in the intensity for the negative ellipticity at 245 nm and an increase in the positive ellipticity band at 275 nm (Fig. 11). These results suggest that interaction of **1**, **2** and **4** did not bring about any conformational changes in CT–DNA while **3** perturbed the stacking interaction as well as the right handed helicity of CT–DNA.

DNA cleavage studies

(a) Chemical–induced DNA cleavage

To assess whether the DNA binding properties of the complexes are associated with the chemical nuclease activity, 300 ng of pUC19 DNA was incubated in presence of hydrogen peroxide as an oxidising agent, with different concentration of the complexes (1–300 μM) in 50 mM Tris–HCl buffer (pH 8.0) containing 1% DMF in dark for 1h. Upon gel electrophoresis, complex **1**, **2** and **4** showed slight DNA cleavage activity ranging from ~ 2–10%, whereas complex **3**, exhibited a maximum chemical nuclease activity of ~ 60% at complex concentration of 100 μM (Fig. 12 and Fig. 13). This enhanced chemical nuclease activity of **3** can be possibly rationalized on the basis of its higher binding affinity towards CT–DNA as observed from the DNA binding studies. Control experiments using the oxidizing agent hydrogen peroxide and the ligands showed that, neither hydrogen peroxide nor the ligands were cleavage active under similar experimental condition (ESI Fig. S10). All the complexes, in the absence of the oxidising agent, were cleavage inactive under dark conditions.

In order to elucidate the probable mechanistic aspect of the chemical–induced DNA cleavage activity by these complexes various inhibitors were used. The chemical−induced DNA cleavage reactions may involve reactive oxygen species (ROS) such as singlet oxygen ($^1O_2$) and hydroxyl radicals (*OH). Therefore, NaN_3 and L–histidine were used as

singlet oxygen quenchers, while KI and D−mannitol were employed as hydroxyl radical quenchers. Complexes **1**, **2** and **4** did not show any appreciable inhibition in the chemical–induced DNA cleavage activity in the presence of the various additives which may be due to the diminished chemical nuclease activity of these complexes (ESI Fig. S11). On the other hand, addition of singlet oxygen quenchers like NaN_3 and L–histidine inhibited the DNA cleavage activity of complex **3** by ~ 6 % and ~ 22 % respectively. Similarly in the presence of the hydroxyl radical scavengers KI and D–mannitol, the chemical nuclease activity of complex **3** was reduced by ~ 14 % and ~ 11 % respectively (Fig. 14). These results suggest that among all the copper complexes, **3** exhibits chemical−induced DNA cleavage activity probably *via* both singlet oxygen and hydroxyl radical pathways.

(b) Photo-induced DNA cleavage

To investigate if the chemical nuclease activity of the complexes were also associated with photo nuclease activity, photo–induced DNA cleavage was carried out with 300 ng pUC19 DNA in the presence and absence of the complexes **1**–**4** (Fig. 15). The extent of DNA cleavage by the complexes was monitored in a concentration dependent manner as shown in Fig. 16. All the complexes (except **4**) showed ~ 10% or more photo−induced DNA cleavage activity at a complex concentration of 10 μM, which ultimately was saturated at a complex concentration of 100 μM. Among the copper(I) complexes, **2** exhibited greater (~ 55 %) photo-induced DNA cleavage activity than **1** (~ 40 %). On the other hand in copper(II) complexes, **3** showed an abruptly higher photo-induced DNA cleavage activity of ~ 80 %, whereas **4** exhibited a minimal DNA cleavage activity of ~ 18 % (Fig. 16). The higher DNA cleavage activity of **3** may be attributed due to its higher binding affinity to DNA as shown in binding studies and also may be because of its solubility in aqueous medium and the presence of quinonoidal group in the thiosemicarbazone ligand coordinated to the metal. Control experiments suggest that neither DMF (1%) nor the ligands showed any photo-induced DNA cleavage activity, which implies that, the ligands or DMF alone are cleavage inactive under similar conditions (ESI Fig. S12).

To understand the mechanistic aspect of the photo nuclease activity of these complexes, we used the same additives as used in exploring the mechanism of chemical nuclease activity. The DNA cleavage reaction involving molecular oxygen can proceed in two mechanistic pathways, namely, a type–II process involving singlet oxygen species ($^1O_2$) or by a photo-redox pathway involving reactive hydroxyl radicals (*OH).[72] In case of copper(I) complexes, the singlet oxygen quenchers, like NaN_3 and L–histidine showed a reduced photo nuclease activity of complex **1** by ~ 9 % and ~ 8 % and of complex **2** by ~ 4 % and ~ 12 % respectively. Similarly the hydroxyl radical scavengers, KI and D–mannitol, exhibited a significant inhibition of photo–induced DNA cleavage activity of complex **1** by ~ 26 % and ~ 13 % and of complex **2** by ~ 19 % and ~ 7 % respectively (Fig. 17 and ESI Fig. S13). While in case of copper(II) complexes, the presence of singlet oxygen quenchers, NaN_3 and L−histidine, decreased the photo nuclease activity of complex **3** by ~ 4 % and ~ 5 % and complex **4** by ~ 3 % and ~ 10 % respectively. Similarly KI and D–mannitol (hydroxyl radical quenchers) showed an inhibition of DNA cleavage activity by ~ 12 % and ~ 28 % for complex **3** and ~ 5 % and ~ 3 % for complex **4** (Fig. 17 and ESI Fig. S12). These results suggest that, **1** & **2** exhibit photo-induced DNA cleavage activity possibly *via* both singlet oxygen and hydroxyl radical pathways while the mechanistic pathway for **3** & **4** cannot be stated with a degree of certainty. Among the two pathways,

hydroxyl radical dominates over the singlet oxygen pathway as the hydroxyl radical scavengers showed higher inhibitory effect than the singlet oxygen quenchers.

Anticancer activity

(a) Inhibition of Cancer Cell Viability

In the present study antiproliferative efficacy of **1**–**4** was assayed by determining the viability of HeLa cells using the MTT assay. The ligands (HL^1, HL^2 and H_2L^4) and metal precursors (CuBr, CuCl & $CuCl_2$) gave IC_{50} values of >200 μM but the other ligand (HL^3) gave IC_{50} values of 98 μM, whereas corresponding complexes **1**–**4** gave values in the range 20–36 μM. The significant decrease in the inhibitory activity for the ligand compared to the metal complex clearly indicates that incorporation of copper in the ligand environment has a marked effect on cytotoxicity. A possible explanation is that by coordination the polarity of the ligand and the central metal ion are reduced through the charge equilibration, which favors permeation of the complexes through the lipid layer of the cell membrane.[73] The present results are consistent with the observation that metal complexes can exhibit greater biological activities than the free ligand.[36]

Comparing the activity of four complexes, the cytotoxic activity follows the order order **3** > **2** > **1** > **4**, which is reflected from the IC_{50} values with dose dependency illustrated in Table 7 & Fig.18. It is remarkable that **3**, having quinonoidal group in the thiosemicarbazone ligand coordinated to the metal is most active. This is in correlation with the fact that the derivatives of quinoline are found to show good biological activities such as antioxidation, antiproliferation, and anti–inflammation.[74,75]

A possible single shot drug for cancer cure has been elusive till date, due to their multiple occurrences in more than a hundred forms and several cases of recurrence of cancer post chemotherapy and surgery are well known. Interestingly, equating the efficacy of our synthesized novel copper compounds against the presently available common chemo drugs sold to the patients, we found out that Cisplatin, Gefitinib, Gemcitabine, 5–Florouracil, Vinorelbine had an IC_{50} of 13μM, 20μM, 35μM, 40 μM and 48μM respectively on HeLa cells, under conditions similar to our experiment.[76] These findings elucidate a positive revelation about the potential aspect of our copper compounds as future neoplastic precursor drug candidates.

(b) Nuclear Staining Assay

To investigate the apoptotic potential of test compounds in HeLa cells, DAPI staining was performed. Chromatin condensation during the process of apoptosis (type I programmed cell death) is a characterizing marker of nuclear alteration. HeLa cells were treated with 30 μM, 25 μM, 15 μM and 30 μM of **1**, **2**, **3** and **4** respectively. All the doses were given below the calculated IC_{50} and the cells were incubated for 24h before DAPI nuclear staining assay. Control cells hardly showed any sort of condensation in comparison to the test compound's activity (as shown in Fig. 19), when the cells were examined under fluorescent microscope, DAPI filter. All images clearly demonstrate the brightly condensed chromatin bodies and the nuclear blebbings as marked by arrows in the figure. The drug treated groups besides showing nuclear changes also revealed a shrinking morphology, which is another important hallmark of apoptosis.

Conclusion

The following are the salient observations and findings of this work:

a) Two Cu(I) complexes **1** $[Cu(L^1)(PPh_3)_2Br]\cdot CH_3CN$ & **2** $[Cu(L^2)(PPh_3)_2Cl]\cdot DMSO$ and two Cu(II) complexes **3** $[(Cu_2L^3{}_2Cl)_2(\mu\text{–}Cl)_2]\cdot 2H_2O$ & **4** $[Cu(L^4)(Py)]$ of thiosemicarbazone ligands were synthesized and characterized by structural, analytical, and spectral methods.

b) The copper complexes **1**–**4** showed good DNA binding propensity. Their DNA binding activities were determined using UV–Vis absorption titration, competitive DNA binding fluorescence experiments, thermal denaturation studies and circular dichroism spectroscopy. The experimental results show that the complexes interact with CT–DNA probably by groove binding mode, with binding constants ranging from 10^4–10^5 M^{-1}. The competitive DNA binding fluorescence experiments suggest that among all the complexes, **3** showed highest quenching constant (Ksv) and K_{app} values.

c) Among all the complexes, **3** displayed significant chemical nuclease activity in presence of hydrogen peroxide of ~ 60 %. All the complexes showed good photo–induced cleavage of pUC19 supercoiled plasmid DNA with complex **3** showing the highest photo induced DNA cleavage activity of ~ 80%.

d) The results from the mechanistic study suggested that, the chemical nuclease activity of complex **3** and the photo nuclease activity of complex **1**–**2** proceeds probably by both singlet oxygen and hydroxyl radical pathways.

e) In addition, the *in vitro* antiproliferative activity of complexes **1**–**4** against HeLa cell line was assayed. The cytotoxicity of the complexes is affected by the various functional groups attached to the thiosemicarbazone derivative whereby **3** was particularly potent against the cells tested.

f) The results of pharmacological activity of the copper complexes reported in this paper reveals that the compound **3** shows the highest activity, which may be due to its solubility in aqueous medium and the presence of quinonoidal group in the thiosemicarbazone ligand coordinated to the metal.

g) The results obtained from the present copper complexes are of importance for the development of metal–based agents for anti–cancer applications. Further work is in progress to better identify the mechanism of action and to prepare more potent related compounds for the treatment of cancer.

Acknowledgements

The authors thank the reviewers for their comments and suggestions, which were helpful in preparing the revised version of the manuscript. Funding for this research was provided by Department of Science and Technology, Govt. of India [Grant No. SR/FT/CS–016/2008 (R.D.) & Grant SR/FT/CS–010/2009 (R.A.)] and Council of Scientific and Industrial Research, India [grant 37(1535)/12/EMR–II) (A.B.)]. R.D. thanks Prof. S.K. Chattopadhyay, Indian Institute of Engineering Science and Technology, Shibpur, for electrochemical studies & fruitful discussions. S.B. gratefully acknowledges the Council of Scientific and Industrial Research, New Delhi, India, for the award of senior research fellowship Grant 9/983(0012)2k13–EMR–I. A.K.P. acknowledges the receipt of ICMR, India grant 45/25/2012–Bio/BMS for providing fellowship.

Notes and references

Corresponding Authors

E-mail: r_acharyya@yahoo.co.in (R. Acharyya)

Tel.: + (91) 661 246 3657; Fax: + (91) 661 246 2022

E-mail: rupamdinda@nitrkl.ac.in (R. Dinda);

Tel.: + (91) 661 246 2657; Fax: + (91) 661 246 2022

†Electronic supplementary information (ESI) available (Table S1, Figs S1−S13): CCDC 1002349, 1002348, 1002351 and 1002350 contain the supplementary crystallographic data for complex **1**, **2**, **3** and **4** respectively. For ESI and crystallographic data in CIF format see DOI: XXXXX

1 T. Boulikas and M. Vougiouka, *Oncol. Rep.,* 2003, **10**, 1663.

2 E. Wong and C. M. Giandomenico, *Chem. Rev.,* 1999, **99**, 2451.

3 M. Galanski, V. B. Arion, M. A. Jakupec and B. K. Keppler, *Curr. Pharm. Des.,* 2003, **9**, 2078.

4 D. Wang and S. J. Lippard, *Nat. Rev. Drug Discovery,* 2005, **4**, 307.

5 A. M. Angeles-Boza, P. M. Bradley, P. K. L. Fu, S. E Wicke, J. Bacsa, K. M Dunbar and C. Turro, *Inorg. Chem.,* 2004, **43**, 8510.

6 B. Rosenberg, L. VamCamp, J. E. Trosko and V. H. Mansour, *Nature*, 1969, **222**, 385.

7 Z. Wu, Q. Liu, X. Liang, X. Yang, N. Wang, X. Wang, H. Sun, Y. Lu and Z. Guo, *J. Biol. Inorg. Chem.*, 2009, **14**, 1313.

8 D. S. Raja, N. S. P. Bhuvanesh and K. Natarajan, *Dalton Trans*., 2012, **41**, 4365.

9 P. J. Bednarski, F. S. Mackay and P. J. Sadler, *Anti-Cancer Agents Med. Chem.*, 2007, **7**, 75.

10 S. Sharma, S. K. Singh, M. Chandra and D. S. Pandey, *J. Inorg. Biochem.*, 2005, **99**, 458.

11 C. Metcalfe and J. A. Thomas, *Chem. Soc. Rev.*, 2003, **32**, 215.

12 C. M. Chang, V. J. Klema, B. J. Johnson, M. Mure, J. P. Klinman, and C. M. Wilmot, *Biochemistry*, 2010, **49**, 2540.

13 E. I. Solomon, P. Chen, M. Metz, Sang-Kyu Lee, and A. E. Palmer, *Angew. Chem., Int. Ed.*, 2001, **40**, 4570.

14 P. Wojciech and M. D. J. D. Nicholas, *BBA-Protein Struct. M.*, 1985, **828**, 130.

15 J. A. Tainer, E. D. Getzoff, J. S. Richardson and D. C. Richardson, *Nature*, 1983, **306**, 284.

16 Y. Matoba, T. Kumagai, A. Yamamoto, H. Yoshitsu, and M. Sugiyama, *J. Biol. Chem.*, 2006, **281**, 8981.

17 J. K. Barton, *Bioinorganic Chemistry*, in: I. Bertini, H. B. Grey, S. J. Lippard and J. S. Valentine (Eds.), University Science Book, Mill Valley, 1994, p. 455.

18 (a) C. Santini, M. Pellei, V. Gandin, M. Porchia, F. Tisato and C. Marzano, *Chem. Rev.*, 2014, **114**, 815. (b) A. N. Kate, A. A. Kumbhar, A. A. Khan, P. V. Joshi and V. G. Puranik, *Bioconjugate Chem.*, 2014, **25**, 102. (c) D. S. Raja, N. S. P. Bhuvanesh and K. Natarajan, *Inorg. Chem.*, 2011, **50**, 12852. (d) M. A. Cater, H. B. Pearson, K. Wolyniec, P. Klaver, M. Bilandzic, B. M. Paterson, A. I. Bush, P. O. Humbert, S. L. Fontaine, P. S. Donnelly and Y. Haupt, *ACS Chem. Biol.,* 2013, **8**, 1621.

19 (a) J. Easmon, G .Purstinger, G. Heinisch, T. Roth, H. H. Fiebig, W. Holzer, W. Jager, M. Jenny and J. Hofmann, *J. Med. Chem.*, 2001, **44**, 2164. (b) P. Jutten, W. Schumann, A. Hartl, H. M. Dahse and U. Grafe, *J. Med. Chem.*, 2007, **50**, 3661. (c) D. C. Greenbaum, Z. Mackey, E. Hansell, P. Doyle, J. Gut, C. R. Caffrey, J. Lehrman, P. J. Rosenthal, J. H. McKerrow and K. Chibale, *J. Med. Chem.*, 2004, **47**, 3212.

20 R. W Brockman, J. R. Thomson, M. J. Bell and H. E. Skipper, *Cancer Res.*, 1956, **16**, 167.

21 M. B. Ferrari, F. Bisceglie, C. Casoli, S. Durot, I. M. Badarau, G. Pelosi, E. Pilotti, S. Pinelli and P. Tarasconi, *J. Med. Chem.*, 2005, **48**, 1671.

22 D. R. Richardson, P. C. Sharpe, D. B. Lovejoy, D. Senaratne, D. S. Kalinowski, M. Islam and P. V. Bernhardt, *J. Med. Chem.*, 2006, **49**, 6510.

23 J. A. Ludwig, G. Szakacs, S. E. Martin, B. F. Chu, C. Cardarelli, Z. E. Sauna, N. J. Caplen, H. M. Fales, S. V. Ambudkar, J. N. Weinstein and M. M. Gottesman, *Cancer Res.*, 2006, **66**, 4808.

24 D. S. Kalinowski, Y. Yu, P. C. Sharpe, M. Islam, Y. T. Liao, D. B. Lovejoy, N. Kumar, P. V. Bernhardt and D. R. Richardson, *J. Med. Chem.*, 2007, **50**, 3716.

25 J. Chen, Y. W. Huang, G. Liu, Z. Afrasiabi, E. Sinn, S. Padhye and Y. Ma, *Toxicol. Appl. Pharmacol.*, 2004, **197**, 40.

26 (a) D. S. Raja, G. Paramaguru, N. S. P. Bhuvanesh, J. H. Reibenspies, R. Renganathan and K. Natarajan, *Dalton Trans.*, 2011, **40**, 4548. (b) P. J. Jansson, P. C. Sharpe, P. V. Bernhardt and D. R. Richardson, *J. Med. Chem.*, 2010, **53**, 5759. (c) S. Adsule, V. Barve, D. Chen, F. Ahmed, Q. P. Dou, S. Padhye and F. H. Sarkar, *J. Med. Chem.*, 2006, **49**, 7242. (d) H. Huang, Q. Chen, X. Ku, L. Meng, L. Lin, X. Wang, C. Zhu, Y. Wang, Z. Chen, M. Li, H. Jiang, K. Chen, J. Ding, and H. Liu, *J. Med. Chem.,* 2010, **53**, 3048.

27 D. X. West, I. H. Hall, K. G. Rajendran and A. E. Liberta, *Anti-cancer Drugs*, 1993, **4**, 231.

28 A. I. Matesanz, C. Joie and P. Souza, *Dalton Trans.*, 2010, **39**, 7059.

29 a) S. Padhye, Z. Afrasiabi, E. Sinn, J. Fok, K. Mehta and N. Rath, *Inorg. Chem.*, 2005, **44**, 1154. b) Z. Afrasiabi, E. Sinn, W. Lin, Y. Ma, C. Campana and S. Padhye, *J. Inorg. Biochem.*, 2005, **99**, 1526.

30 (a) P. Kalaivani, R. Prabhakaran, P. Poornima, F. Dallemer, K. Vijayalakshmi, V. V. Padma and K. Natarajan, *Organometallics*, 2012, **31**, 8323. (b) L. Otero, M. Vieites, L. Boiani, A. Denicola, C. Rigol, L. Opazo, C. Olea-Azar, J. D. Maya, A. Morello, R. L. K. Siegel, O. E. Piro, E. Castellano, M. González, D. Gambino and H. Cerecetto, *J. Med. Chem.*, 2006, **49**, 3322. (c) M. Baldini, M.B. Ferrari, F. Bisceglie, P.P. Dall'Aglio, G. Pelosi, S. Pinelli and P. Tarasconi, *Inorg. Chem.*, 2004, **43**, 7170. (d) M. Baldini, M. B. Ferrari, F. Bisceglie, G. Pelosi, S. Pinelli and P. Tarasconi, *Inorg. Chem.*, 2003, **42**, 2049. (e) P. Kalaivani, R. Prabhakaran, E. Ramachandran, F. Dallemer, G. Paramaguru, R. Renganathan, P. Poornima, V. V. Padma and K. Natarajan, *Dalton Trans.*, 2012, **41**, 2486. (f) K. Sampath, S. Sathiyaraj and C. Jayabalakrishnan, *Med. Chem. Res.*, 2014, **23**, 958. (g) J. G. D. Silva, A. A. R. Despaigne, S. R. W. Louro, C. C. Bandeira, E. M. Souza-Fagundes and H. Beraldo, *Eur. J. Med. Chem.*, 2013, **65**, 415. (h) E. Ramachandran, S. P. Thomas, P. Poornima, P. Kalaivani, R. Prabhakaran, V. V. Padma and K. Natarajan, *Eur. J. Med. Chem.*, 2012, **50**, 405. (i) J. Lu, H. Guo , X. Zeng , Y. Zhang, P. Zhao, J. Jiang and L. Zang, *J. Inorg. Biochem.*, 2012, **112**, 39.

31 Z. Afrasiabi, E. Sinn, S. Padhye, S. Dutta, S. Padhye, C. Newton, C. E. Anson and A. K. Powell , *J. Inorg. Biochem.*, 2003, **95**, 306.

32 E. M. Jouad, G. Larcher, M. Allain, A. Riou, G. M. Bouet, M. A. Khan and X. D. Thanh, *J. Inorg. Biochem.*, 2001, **86**, 565.

33 S. Sharma, F. Athar, M. R. Maurya, F. Naqvi and A. Azam, *Eur. J. Med. Chem.*, 2005, **40**, 557.

34 T. Wang and Z. Guo, *Curr. Med. Chem.*, 2006, **13**, 525.

35 A. Gaál, G. Orgován, Z. Polgári, A. Réti, V. G. Mihucz, S. Bősze, N. Szoboszlai and C. Streli, *J. Inorg. Biochem.*, 2014, **130**, 52.

36 T. Rosu, E. Pahontu, S. Pasculescu, R. Georgescu, N. Stanica, A. Curaj, A. Popescu and M. Leabu, *Eur. J. Med. Chem.*, 2010, **45**, 1627.

37 D. Palanimuthu, S. V. Shinde, K. Somasundaram and A. G. Samuelson, *J. Med. Chem.*, 2013, **56**, 722.

38 D. S. Raja, N. S. P. Bhuvanesh and K. Natarajan, *Eur. J. Med. Chem.*, 2011, **46**, 4584.

39 F. Bisceglie, M. Baldini, M. B. Ferrari, E. Buluggiu, M. Careri, G. Pelosi, S. Pinelli and P. Tarasconi, *Eur. J. Med. Chem.*, 2007, **42**, 627.

40 Z. C. Liu, B. D. Wang, Z. Y. Yang, Y. Li, D. D. Qin and T. R. Li, *Eur. J. Med. Chem.*, 2009, **44**, 4477.

41 Z. Afrasiabi, E. Sinn, P. P. Kulkarni, V. Ambike, S. Padhye, D. Deobagakar, M. Heron, C. Gabbutt, C.E. Anson and A.K. Powell, *Inorg. Chim. Acta*, 2005, **358**, 2023.

42 A. R. Cowley, J. R. Dilworth, P. S. Donnelly and J. M. White, *Inorg. Chem.*, 2006, **45**, 496.

43 M. C. Rodriguez-Arguelles, Lopez-Silva Ee, J. Sanmartin, P. Pelagatti and F. Zami, *J. Inorg. Biochem.*, 2005, **99**, 2231.

44 L. J. Ashfield, A. R. Cowley, J. R. Dilworth and P. S. Donnelly, *Inorg. Chem.*, 2004, **43**, 4121.

45 T. S. Lobana, S. Khanna, R. J. Butcher, A. D. Hunter and M. Zeller, *Polyhedron*, 2006, **25**, 2755.

46 P. M. Krishna and K. H. Reddy, *Inorg. Chim. Acta*, 2009, **362**, 4185.

47 (a) S. P. Dash, S. Pasayat, Saswati, H. R. Dash, S. Das, R. J. Butcher and R. Dinda, *Polyhedron*, 2012, **31**, 524. (b) S. Pasayat, S. P. Dash, Saswati, P. K. Majhi, Y. P. Patil, M. Nethaji, H. R. Dash, S. Das and R. Dinda, *Polyhedron*, 2012, **38**, 198. (c) Saswati, R. Dinda, C. S. Schmiesing, E. Sinn, Y. P. Patil, M. Nethaji, H. Stoeckli-Evans and R. Acharyya, *Polyhedron*, 2013, **50**, 354. (d) S. P. Dash, S. Pasayat, S. Bhakat, S. Roy, R. Dinda, E. R. T. Tiekink, S. Mukhopadhyay, S. K. Bhutia, M. R. Hardikar, B. N. Joshi, Y. P. Patil and M. Nethaji, *Inorg. Chem.*, 2013, **52**, 14096. (e) S. P. Dash, A. K. Panda, S. Pasayat, R. Dinda, A. Biswas, E. R. T. Tiekink, Y. P. Patil, M. Nethaji, W. Kaminsky, S. Mukhopadhyay and S. K. Bhutia, *Dalton Trans.*, 2014, **43**, 10139.

48 Part 1: S. Ghosh and S. Purohit, *Indian J. Chem., Sect. A: Inorg., Bio-inorg., Phys., Theor. Anal. Chem.*, 1987, **26A**, 131.

49 T. S. Lobana, Rekha, R. J. Butcher, A. Castineiras, E. Bermejo and P. V. Bharatam, *Inorg. Chem.*, 2006, **45**, 1535.

50 E. Blanc, D. Schwarzenbach and H. D. Flack, *J. Appl. Crystallogr.*, 1991, **24**, 1035.

51 Bruker, *SADABS*, *SAINT, SHELXTL and SMART*, Bruker AXS Inc., Madison, Wisconsin, SA, 2003.

52 G. M. Sheldrick, *Acta Crystallogr., Sect. A: Found. Crystallogr.*, 2008, **64**, 112.

53 P. Krishnamoorthy, P. Sathyadevi, A. H. Cowley, R. R. Butorac and N. Dharmaraj, *Eur. J. Med. Chem.*, 2011, **46**, 3376.

54 W. M. Dai, K. W. Lai, A. Wu, W. Hamaguchi, M. Y. Lee, L. Zhou, A. Ishii and S. Nishimoto, *J. Med. Chem.*, 2002, **45**, 758.

55 S. Mukhopadhyay, P. K. Panda, B. Behera, C. K. Das, M. K. Hassan, D. N. Das, N. Sinha, A. Bissoyi, K. Pramanik, T. K. Maiti and S. K. Bhutia, *Food Chem. Toxicol*., 2014, **64**, 369.

56 S. Mukhopadhyay, P. K. Panda, D. N. Das, N Sinha, B. Behera, T. K. Maiti and S. K. Bhutia, *Acta Pharmacol. Sin.,* 2014, **35**, 814.

57 T. S. Lobana, P. K. Bhatia and E. R. T. Tiekink, *J. Chem. Soc., Dalton Trans.,* 1989, 749.

58 V. Philip, V. Suni, M. R. P. Kurup and M. Nethaji, *Polyhedron*, 2006, **25**, 1931.

59 A. Sreekanth and M. R. P. Kurup, *Polyhedron,* 2003, **22**, 3321.

60 T. S. Lobana, P. Kumari, G. Hundal and R. J. Butcher, *Polyhedron*, 2010, **29**, 1130.

61 S. Datta, D. K. Seth, R. J. Butcher and S. Bhattacharya, *Inorg. Chim. Acta*, 2011, **377**, 120.

62 V. M. Leovac, G. A. Bogdanović, .S. Jovanović, L. Joksović, V. Marković, M. D. Joksović, S. M. Denčić, A. Isaković, I. Marković, F. W. Heinemann, S. Trifunović and I. Đalović, *J. Inorg. Biochem.*, 2011, **105**, 1413.

63 M. Nirmala, R. Manikandan, G. Prakash and P. Viswanathamurthi, *Appl. Organomet. Chem.*, 2014, **28**, 18.

64 P. Chakraborty, J. Adhikary, B. Ghosh, R. Sanyal, S. K. Chattopadhyay, A. Bauzá, A. Frontera, E. Zangrando and D. Das, *Inorg. Chem.,* 2014, **53**, 8257.

65 (a) C. R. Kowol, P. Heffeter, W. Miklos, L. Gille, R. Trondl, L. Cappellacci, W. Berger and B. K. Keppler, *J. Biol. Inorg. Chem.*, 2012, **17**, 409.(b) Y. H. Zhou, J. Tao, D. L. Sun, L. Q. Chen, W. G. Jia, Y. Cheng, *Polyhedron,* 2015, **85**, 849–856. (c) S. Naskar, S. Naskar, H. M. Figge, W. S. Sheldrick, M. Corbella, J. Tercero, S. K. Chattopadhyay, *Polyhedron*, 2012, **35,** 77–86.

66 (a) D. Mishra, S. Naskar, M. G. B. Drew and S. K. Chattopadhyay, *Inorg. Chim. Acta*, 2006, **359**, 585. (b) P. Paul, D. K. Seth, M. G. Richmond and S. Bhattacharya, *RSC Adv*., 2014, **4**, 1432.

67 P. Kumar, S. Gorai, M. K. Santra, B. Mondal and D. Manna, *Dalton Trans.*, 2012, **41**, 7573.

68 A. K. Patra, T. Bhowmick, S. Ramakumar, M. Nethaji and A. R. Chakravarty, *Dalton Trans*., 2008, **48**, 6966.

69 Y. An, S. D. Liu, S. Y. Deng, L. N. Ji and Z. W. Mao, *J. Inorg. Biochem.*, 2006, **100**, 1586.

70 S. Banerjee, A. Hussain, P. Prasad, I. Khan, B. Banik, P. Kondaiah and A. R. Chakravarty, *Eur. J. Inorg. Chem.*, 2012, 3899.

71 L. Li, Q. Guo, J. Dong, T. Xu and J. Li, *J. Photochem. Photobiol., B*, 2013, **125**, 56.

72 P. K. Sasmal, S. Saha, R. Majumdar, S. De, R. R. Dighe and A. R. Chakravarty, *Dalton Trans.*, 2010, **39**, 2147.

73 P. G. Avaji, C. H. V. Kumar, S. A. Patil, K. N. Shivananda and C. Nagaraju, *Eur. J. Med. Chem.*, 2009, **44**, 3552.

74 I. R. Canelón and P. J. Sadler, *Inorg. Chem.*, 2013, **52**, 12276.

75 J. S. Casas, M. S. G. Tasende and J. Sordo, *Coord. Chem. Rev.*, 2000, **209**, 197.

76 M. Ahmed and K. Jamil, *Biol. Med*., 2011, **3**, 60.

Table 1 Crystal and Refinement Data of Complexes **1**–**4**

Compound	**1**	**2**	**3**	**4**
Formula	$C_{56}H_{47}BrClCuN_4P_2S$	$C_{56}H_{50}BrClCuN_3OP_2S_2$	$C_{44}H_{40}Cl_4Cu_4N_{16}S_4O_2$	$C_{19}H_{15}CuFN_4OS$
M	1048.88	1085.95	1349.12	429.95
Crystal system	Triclinic	Triclinic	Triclinic	Monoclinic
Space group	P -1	P -1	P -1	P 21/c
a(Å)	9.4984(4)	9.6604(5)	8.9472(15)	13.3041(5)
b(Å)	13.1221(5)	13.1537(6)	9.8129(16)	5.8394(2)
c(Å)	20.6583(9)	20.3412(10)	14.928(2)	23.1869(9)
α (°)	100.185(3)	99.305(4)	85.086(3)	90
β (°)	95.359(3)	94.696(4)	72.973(3)	102.115(2)
γ (°)	96.502(3)	93.570(4)	80.782(3)	90
V(Å^3)	2500.96(18)	2534.7(2)	1236.0(4)	1761.22(11)
Z	2	2	1	4
D_{calc}(Mg.cm^{-3})	1.393	1.423	1.813	1.621
F(000)	1076	1116	680	876
μ(Mo-Kα)(mm^{-1})	1.436	1.460	2.142	1.386
max./min.trans.	0.9460 and 0.8576	0.8921 and 0.7026	0.9873 and 0.8343	0.9728 and 0.7787
2θ(max)(°)	25.00	25.00	21.99	30.5
Reflections collected	48158/8790	48925/8938	8969/4328	33365/5407
/ unique	[R(int) = 0.0383]	[R(int) = 0.0576]	[R(int) = 0.0406]	[R(int) = 0.0410]
R_1[I>2σ(I)]	R1 = 0.0301,	R1 = 0.0477,	R1 = 0.0743,	R1 = 0.0345,
	wR2 = 0.0788	wR2 = 0.1269	wR2 = 0.1738	wR2 = 0.0796
wR_2[all data]	R1 = 0.0353,	R1 = 0.0754,	R1 = 0.1261,	R1 = 0.0581,
	wR2 = 0.0814	wR2 = 0.1400	wR2 = 0.1963	wR2 = 0.0885
S[goodness of fit]	1.040	1.034	1.018	1.015
min./max. res.	0.788 and –0.755	0.824 and –0.867	2.059 and –0.897	0.315 and –0.295
(e.Å^{-3})				

Table 2 Selected Bond Distances (Å) and Bond Angles (°) for $[Cu(L^1)(PPh_3)_2Br]\cdot CH_3CN$ (**1**) and $[Cu(L^2)(PPh_3)_2Cl]\cdot DMSO$ (**2**)

	Complex (**1**)	Complex (**2**)
	Bond Distance	
Cu(1)-S(1)	2.401(7)	2.387(1)
Cu(1)-P(1)	2.277(6)	2.274(1)
Cu(1)-P(2)	2.290(7)	2.295(1)
Br(1)-Cu(1)	2.517(4)	–
Cl(1)-Cu(1)	–	2.374(1)
	Bond Angles	
P(2)-Cu(1)-P(1)	124.51(2)	122.72(4)
P(2)-Cu(1)-S(1)	109.26(2)	107.07(4)
P(1)-Cu(1)-S(1)	104.48(2)	105.19(4)
P(2)-Cu(1)-Br(1)	108.41 (2)	–
P(2)-Cu(1)-Cl(1)	–	108.07(4)
P(1)-Cu(1)-Br(1)	100.29(2)	–
P(1)-Cu(1)-Cl(1)	–	104.81(4)
S(1)-Cu(1)-Br(1)	108.97(2)	–
Cl(1)-Cu(1)-S(1)	–	108.35(4)

Table 3 Selected Bond Distances (Å) and Bond Angles (°) for $[(Cu_2L^3{}_2Cl)_2(\mu\text{–}Cl)_2]\cdot 2H_2O$ (**3**) & $[Cu(L^4)(Py)]$ (**4**)

	Complex (**3**)	Complex (**4**)
	Bond Distance	
Cu(1)-Cl(1)	2.253(3)	–
Cu(1)-O(1)	–	1.906 (2)
Cu(1)-S(1)	2.304(3)	2.247(6)
Cu(1)-S(2)	2.715(2)	–
Cu(1)-N(3)	1.975(7)	1.932(1)
Cu(1)-N(4)	2.107(7)	2.013(1)
Cu(2)-Cl(2)	2.290(2)	–
Cu(2)-S(2)	2.303(2)	–
Cu(2)-N(7)	1.973(6)	–
Cu(2)-N(8)	2.146(6)	–
Cu(2)-Cl(2)1	2.691(2)	–
	Bond Angles	
Cl(1)-Cu(1)-S(1)	92.60(1)	–
O(1)-Cu(1)-N(3)	–	94.04(7)
Cl(1)-Cu(1)-S(2)	101.30(1)	–
O(1)-Cu(1)-N(4)	–	86.40(7)
Cl(1)-Cu(1)-N(3)	150.60(2)	–
O(1)-Cu(1)-S(1)	–	177.41(5)
Cl(1)-Cu(1)-N(4)	104.10(2)	–
S(1)-Cu(1)-S(2)	94.15(8)	–
S(1)-Cu(1)-N(3)	82.30(2)	85.92(5)
S(1)-Cu(1)-N(4)	161.90(2)	93.72(5)
S(2)-Cu(1)-N(3)	107.90(2)	–
S(2)-Cu(1)-N(4)	89.40(2)	–
N(3)-Cu(1)-N(4)	79.70(3)	178.10(7)
Cl(2)-Cu(2)-S(2)	89.88(8)	–
Cl(2)-Cu(2)-N(7)	171.20(2)	–
Cl(2)-Cu(2)-N(8)	108.60(2)	–
Cl(2)-Cu(2)-Cl(2)1	87.25(7)	–
S(2)-Cu(2)-N(7)	81.60(2)	–

S(2)-Cu(2)-N(8)	155.20(2)	–
Cl(2)1-Cu(2)-S(2)	102.01(9)	–
N(7)-Cu(2)-N(8)	79.20(3)	–
Cl(2)1-Cu(2)-N(7)	96.30(2)	–
Cl(2)1-Cu(2)-N(8)	95.50(2)	–
Cu(2)-Cl(2)-Cu(2)1	92.80(9)	–

Table 4 Electronic spectra for Complexes **1**–**4** in CH_3OH

Complex	λ_{max}/nm (ε/dm^{3}mol^{-1} cm^{-1})
$[Cu(L^1)(PPh_3)_2Br]\cdot CH_3CN$ (**1**)	239(51814), 349(26982)
$[Cu(L^2)(PPh_3)_2Cl]\cdot DMSO$ (**2**)	227(45121), 385(27637)
$[(Cu_2L^3{}_2Cl)_2(\mu\text{–}Cl)_2]\cdot 2H_2O$ (**3**)	230(29790), 306(23258), 364(12917), 448(11768), 676(17788)
$[Cu(L^4)(Py)]$ (**4**)	220(5132), 256(8526), 332(3310), 395(2574), 668(4353)

Table 5 Cyclic voltammetric[a] results for Complexes **1**–**4** at 298 K

Complex	Potentials (V) versus Ag/AgCl				
	Cu(I)/Cu(II)	Cu(I)/Cu(0)	Ligand –centered	Ligand –centered	Cu(II)/Cu(I)
	$E^{a}_{1/2}(\Delta E^{a}_{P})$	E_{pc}	oxidation	reduction	$E^{c/a}_{1/2}(\Delta E^{c/a}_{P})$
			$E^{a}_{1/2}(\Delta E^{a}_{P})$	E_{pc}	
$[Cu(L^{1})(PPh_3)_2Br]\cdot CH_3CN$ (**1**)	0.40(320)	–0.72	0.89(240)	–1.41, –1.63	–
$[Cu(L^{2})(PPh_3)_2Cl]\cdot DMSO$ (**2**)	0.37(326)	–0.70	0.87(156)	–1.45, –1.65	–
$[(Cu_2L^{3}{}_2Cl)_2(\mu\text{–}Cl)_2]\cdot 2H_2O$ (**3**)	–	–	0.88(190)	–1.39, –1.63	–0.62(50)
					0.10(77), 0.36(113),
$[Cu(L^{4})(Py)]$ (**4**)	–	–	0.91(264)	–1.37, –1.61	–0.52(100)

[a]In CH_3CN at a scan rate 100 mV/s. $E_{1/2} = (E_{pa} + E_{pc})/2$, where E_{pa} and E_{pc} are anodic and cathodic peak potentials vs. Ag/AgCl, respectively. $\Delta E_P = E_{pa} - E_{pc.}$

Table 6 DNA binding parameters for the complexes **1**–**4**

Complex	Binding Constant (K_b)[a] (M^{-1})	ΔT_m [b] (°C)	Stern–Volmer Quenching Constant (K_{SV}) (M^{-1})[c]	K_{app} (M^{-1})[d]
1	3.40×10^5	+1.05	3.06×10^3	6.87×10^5
2	1.20×10^5	+1.65	2.22×10^3	6.70×10^5
3	9.60×10^5	+1.83	5.36×10^4	7.34×10^5
4	1.30×10^4	+1.11	1.32×10^3	5.79×10^5

[a]DNA binding constant by UV–vis spectral method. [b]Change in the melting temperature of CT–DNA. [c]Stern–Volmer quenching constant for CT–DNA–EB complex. [d]the apparent DNA binding constant.

Table 7 Cytotoxic scores in HeLa cancer cells for **1**–**4**

Compounds	IC_{50} (μM)
1	33.5±4.67
2	31.5±5.72
3	19.8±3.54
4	36±6.74

Figure Captions

Chart 1 Lists of TSC derivatives exhibiting intense anticancer activities.

Scheme 1 Schematic representation of ligands and synthesis of copper complexes.

Fig. 1 ORTEP diagram of $[Cu(L^1)(PPh_3)_2Br]\cdot CH_3CN$ (**1**) with atom labeling scheme.

Fig. 2 ORTEP diagram of $[Cu(L^2)(PPh_3)_2Cl]\cdot DMSO$ (**2**) with atom labeling scheme.

Fig. 3 ORTEP diagram of $[(Cu_2L^3{}_2Cl)_2(\mu\text{–}Cl)_2]\cdot 2H_2O$ (**3**) with atom labeling scheme.

Fig. 4 ORTEP diagram of $[Cu(L^4)(Py)]$ (**4**) with atom labeling scheme

Fig. 5 Cyclic voltammogram of complex **1**.

Fig. 6 Cyclic voltammogram of complex **3**.

Fig. 7 Cyclic voltammogram of complex **4**.

Fig. 8 Electronic absorption spectra of **1** (a), **2** (b), **3** (c) and **4** (d) (25 μM each) upon the titration of CT–DNA (0–70 μM) in 10 mM Tris–HCl buffer (pH 8.0) containing 1% DMF. Arrow shows the changes in absorbance with respect to an increase in the CT–DNA concentration. The inset shows the linear fit of $[DNA]/(\varepsilon_a - \varepsilon_f)$ vs [DNA] and binding constant (K_b) was calculated using Eq. 1.

Fig. 9 Fluorescence absorption spectra of **1** (a), **2** (b), **3** (c) and **4** (d) (0–60 μM) on the emission intensity of ethidium bromide (2 μM) bound CT–DNA (50 μM) at different concentrations in 10 mM Tris–HCl buffer (pH 8.0) containing 1% DMF. Arrow indicates the effect of increasing concentration of complex on the fluorescence emission of ethidium bromide bound CT–DNA. The inset shows the linear fit of F_0/F *vs* [complex] and Stern–Volmer quenching constant (K_{SV}) was calculated using Eq. 2.

Fig. 10 Derivative plot of thermal denaturation of CT–DNA (100 μM) in absence and presence of **1**–**4** (50 μM). The experiment was done in 10 mM Tris–HCl buffer (pH 8.0) containing 1% DMF. Inset shows the ΔT_m (^oC) of the complexes as compared to CT–DNA.

Fig. 11 Circular dichroism spectra of CT–DNA (50 μM) in the presence and absence of **1**–**4** (20 μM) in 10 mM Tris–HCl buffer (pH 8.0) containing 1% DMF. The path length of the cuvette was 10 mm.

Fig. 12 Gel diagram showing concentration dependent chemical nuclease activity by **1**–**4**; 300ng of SC pUC19 DNA at different concentrations of the complexes [1–300 μM in 50 mM Tris–HCl buffer (pH 8.0) containing 1% DMF] was treated with hydrogen peroxide (0.5mM) in dark for 1 h at 37^{o}C. Lanes 1–9: 1, 2.5, 5.0, 7.5, 10, 50, 75, 100 and 300 μM of **1**–**4**.

Fig. 13 Concentration dependent chemical nuclease activity by **1**–**4**; 300 ng of SC pUC19 DNA at different concentration of the complexes [1–300 μM in 50 mM Tris–HCl buffer (pH 8.0) containing 1% DMF] was treated with hydrogen peroxide (0.5 mM) in dark for 1 h at 37^{o}C. The net DNA cleavage percent was calculated using Eq. 4. Inset shows a bar diagram representation of the net DNA cleavage of different complexes at 10 and 100 μM.

Fig. 14 Chemical nuclease activity of SC pUC19 DNA by **3** in presence of various additives in 50 mM Tris–HCl buffer (pH 8.0) containing 1% DMF. SC pUC19 DNA (300 ng) in the presence of various additives was treated with hydrogen peroxide

(0.5 mM) in dark for 1 h at 37°C with **3** (100 μM). The additive concentrations were: sodium azide (0.5 mM), L–histidine (0.5 mM), KI (0.5 mM) and D–mannitol (0.5 mM).

Fig. 15 Gel diagram showing concentration dependent DNA cleavage by **1**–**4**; 300ng of SC pUC19 DNA at different concentrations of the complexes [1–300 μM in 50 mM Tris–HCl buffer (pH 8.0) containing 1% DMF] was photo–irradiated with UVA at 350 nm for 1 h. Lanes 1–9: 1, 2.5, 5.0, 7.5, 10, 50, 75, 100 and 300 μM of **1**–**4**.

Fig. 16 Concentration dependent DNA cleavage by **1**–**4**; 300 ng of SC pUC19 DNA at different concentration of the complexes [1–300 μM in 50 mM Tris–HCl buffer (pH 8.0) containing 1% DMF] was photo–irradiated with UVA at 350 nm for 1 h. The net DNA cleavage percent was calculated using Eq. 4. Inset shows a bar diagram representation of the net DNA cleavage of different complexes at 10 and 100 μM.

Fig. 17 DNA cleavage of SC pUC19 DNA by **1**–**4** in presence of various additives in 50 mM Tris–HCl buffer (pH 8.0) containing 1% DMF. SC pUC19 DNA (300 ng) in the presence of various additives was photo–irradiated at 350 nm for 1 h with **1**–**4** (100 μM). The additive concentrations were: sodium azide (0.5 mM), L–histidine (0.5 mM), KI (0.5 mM) and D–mannitol (0.5 mM).

Fig. 18 Effect of **1**, **2**, **3** and **4** on cancer cell viability and growth: HeLa cells were treated with different concentrations of the test compounds for 72h and then cell viability was measured by MTT assay. Data reported as the mean±S.D. for $n = 6$ and compared against control by using a Student's *t*–test. (*denotes significance compared to control).

Fig. 19 Study of apoptosis by morphological changes in nuclei of HeLa cells: After treatment, HeLa cells from control and treated group were fixed with 3.7% formaldehyde for 15 min, permeabilized with 0.1% Triton X–100 and stained with 1μg/ml DAPI for 5 min at 37°C. The cells were then washed with PBS and examined by fluorescence microscopy (Olympus IX 71) (200×).

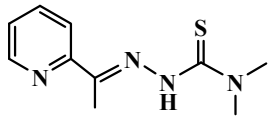

4,4-Dimethyl-2-formylpyridine TSC

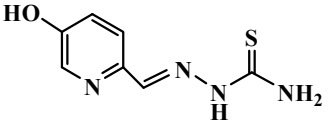

5-hydroxypyridin-2-carboxaldehyde TSC

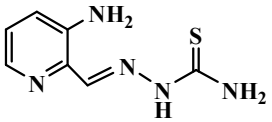

3-Aminopyridine-2-carboxaldehyde TSC

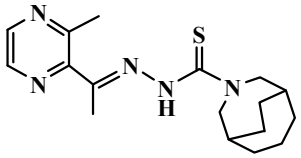

^{4}*N*-Azabicyclo[*3.2.2*]nonane TSC

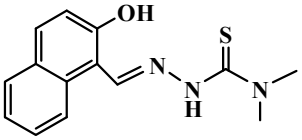

4,4-Dmethyl-2-hydroxy-1-naphthaldehyde TSC

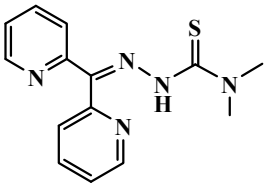

di-2-Pyridylketone-4,4-dimethyl-3 TSC

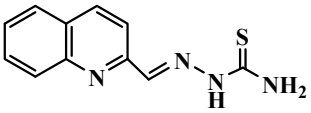

Quinolin-2-carboxaldehyde TSC

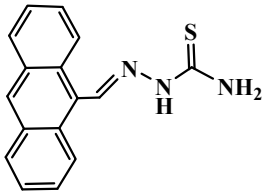

Anthracene-9-carboxaldehyde TSC

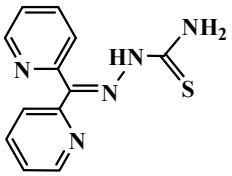

di-2-Pyridylketone TSC

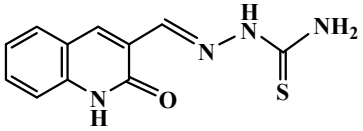

2-Oxo-1,2-dihydroquinoline-3-carbaldehyde TSC

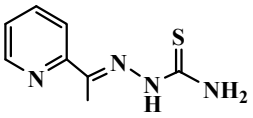

2-Acetylpyridine TSC

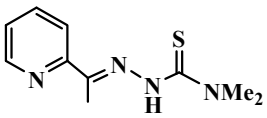

2-Acetylpyridine-4,4-dimethyl-3 TSC

Chart 1

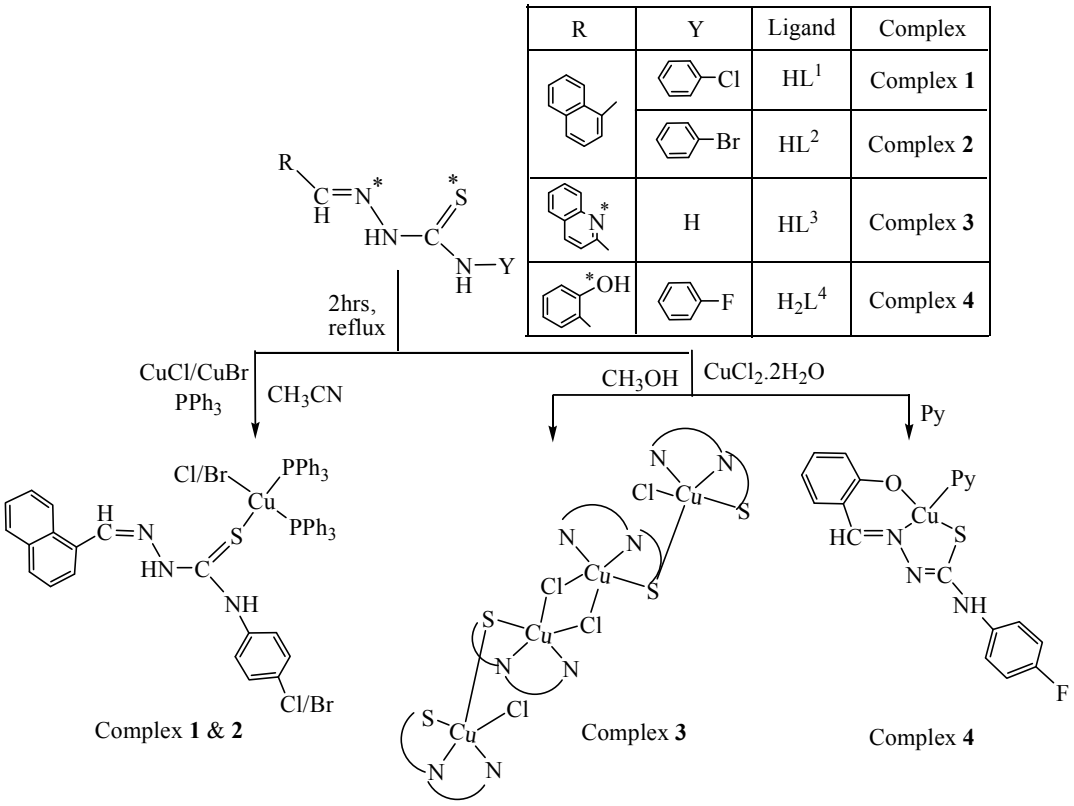

Scheme 1

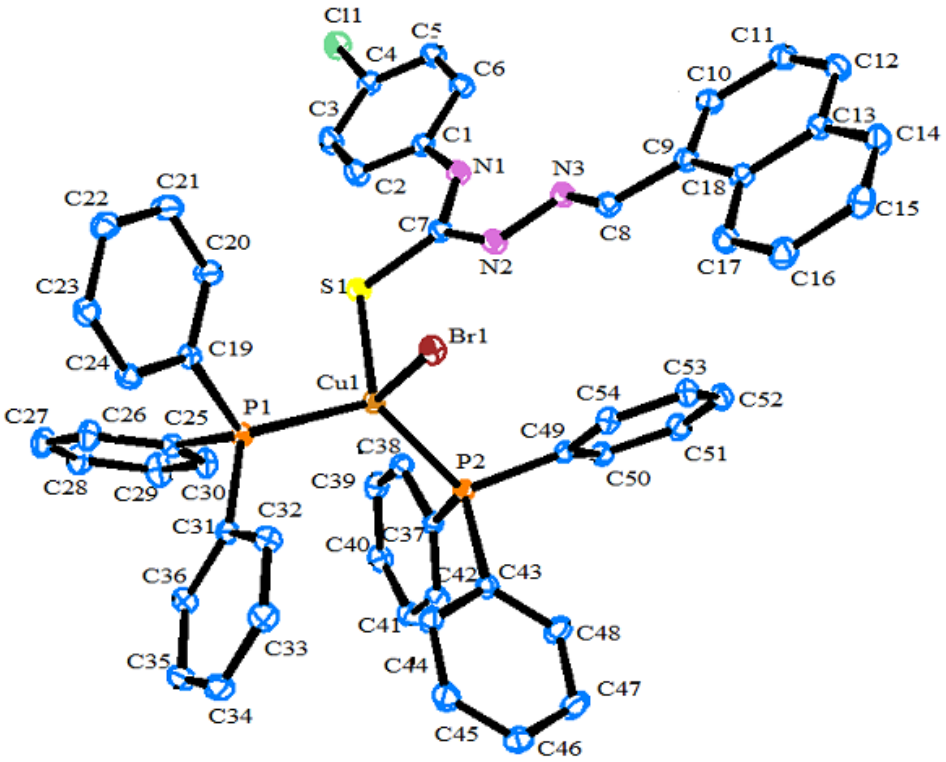

Fig. 1.

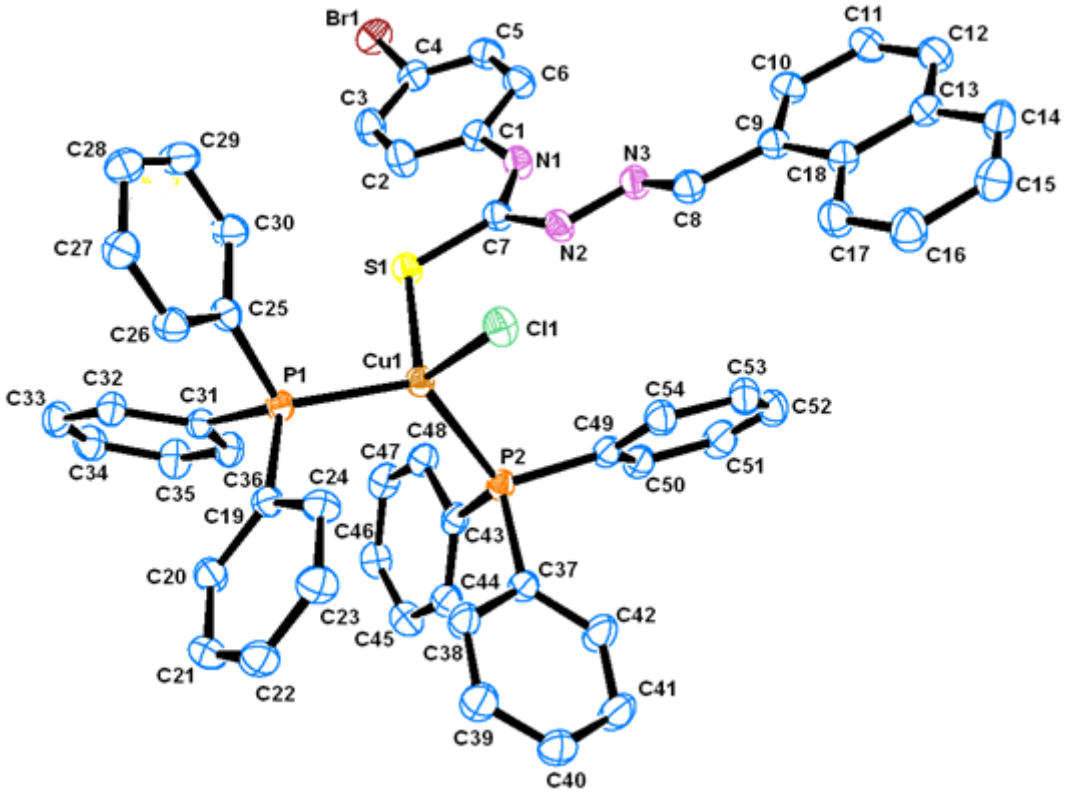

Fig. 2.

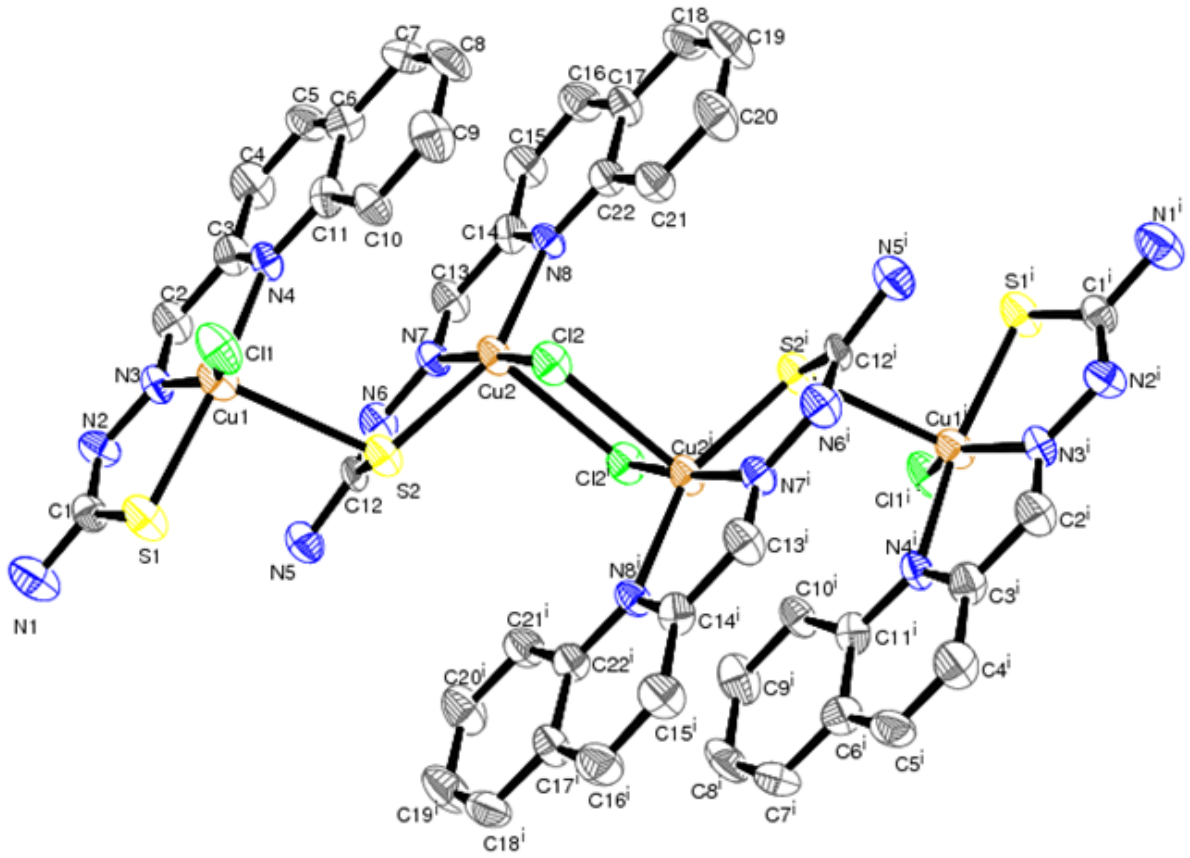

Fig. 3.

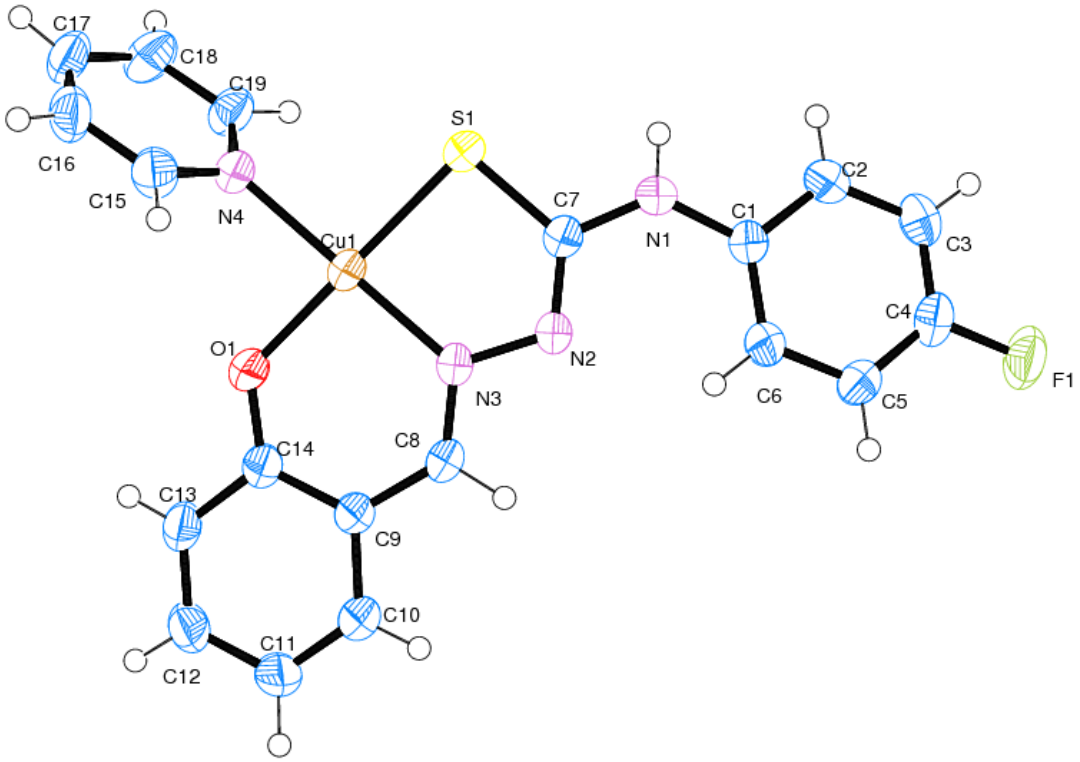

Fig. 4.

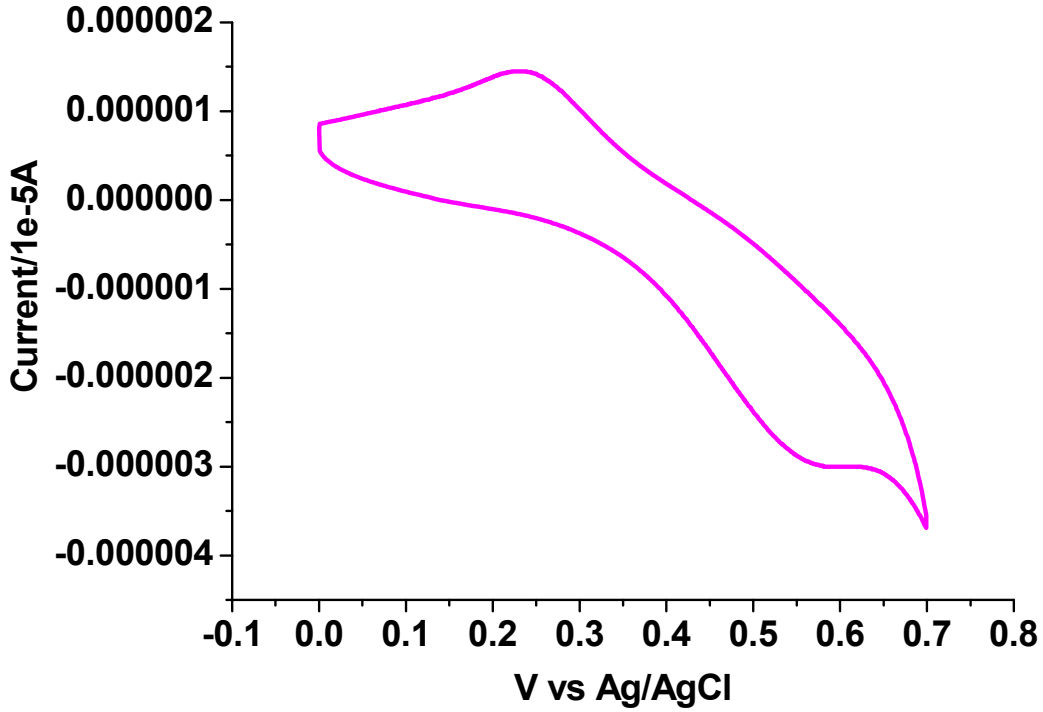

Fig. 5.

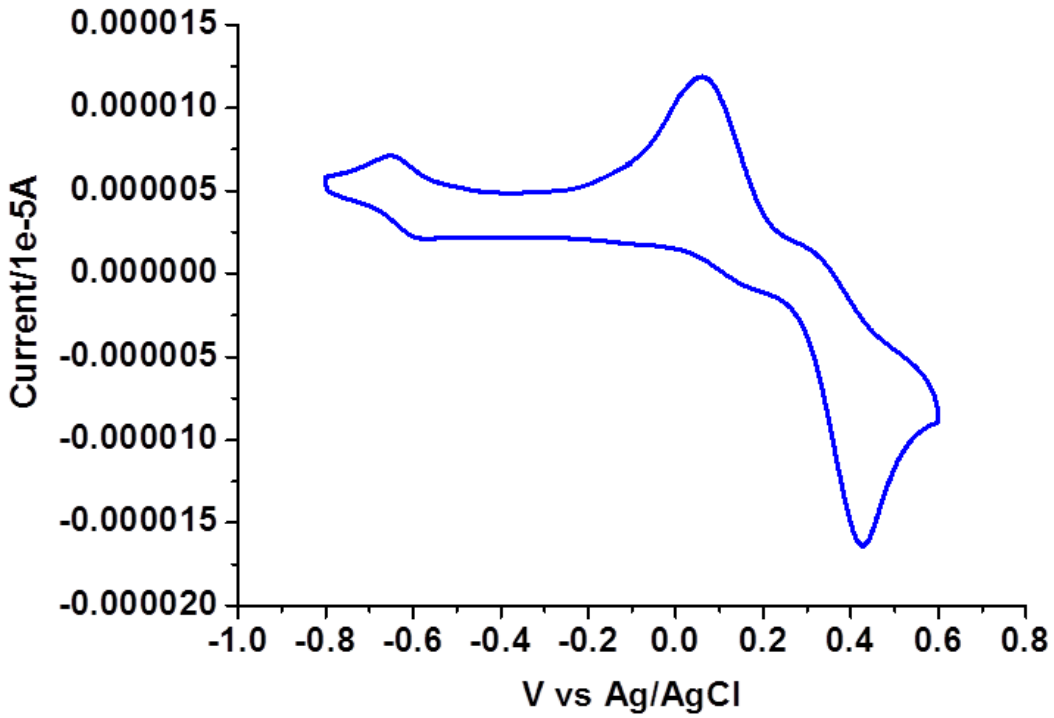

Fig. 6.

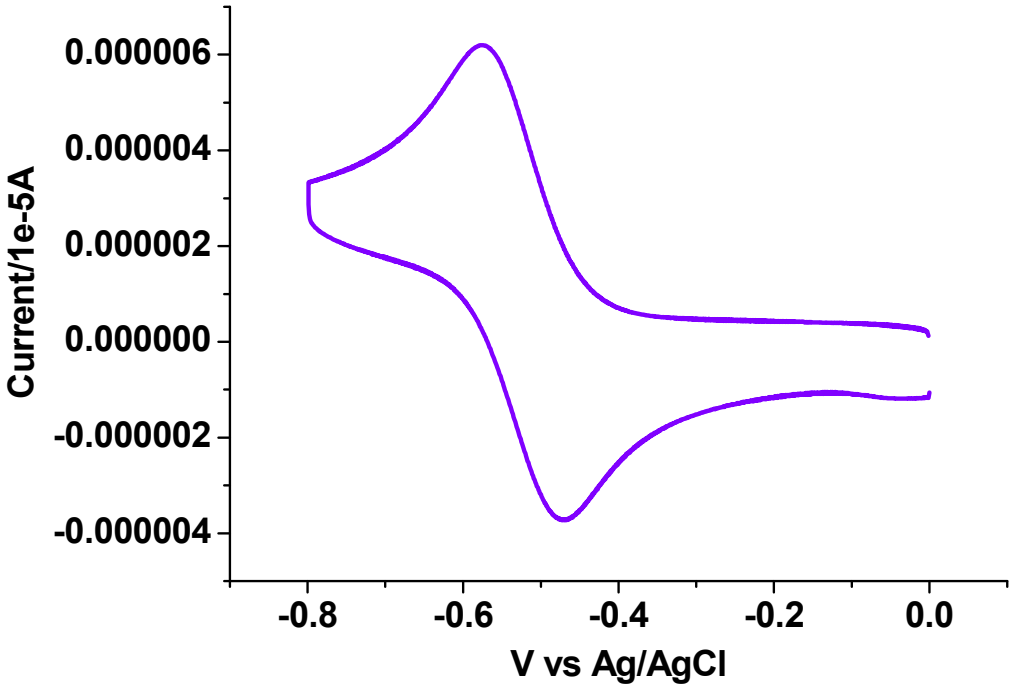

Fig. 7.

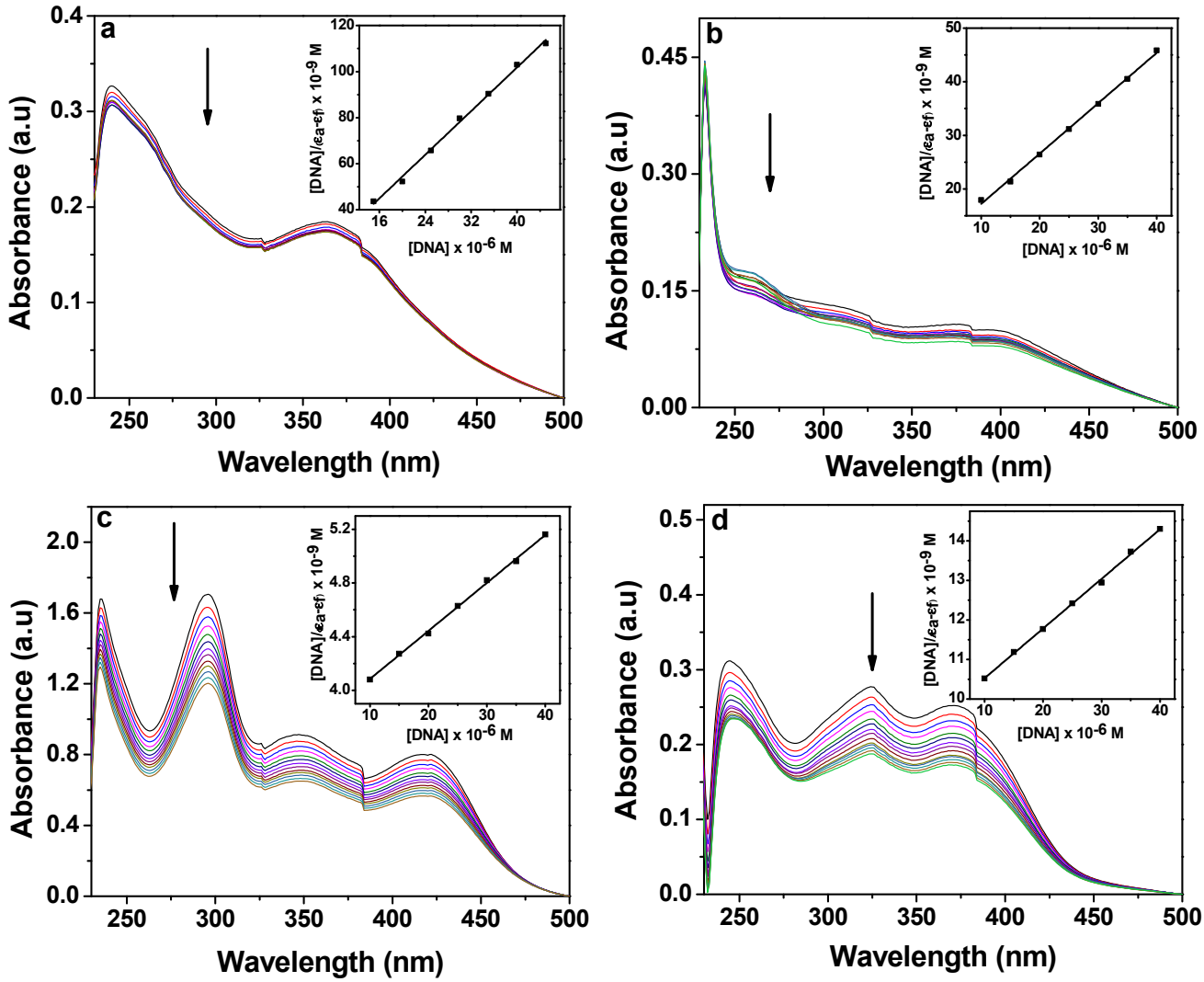

Fig. 8.

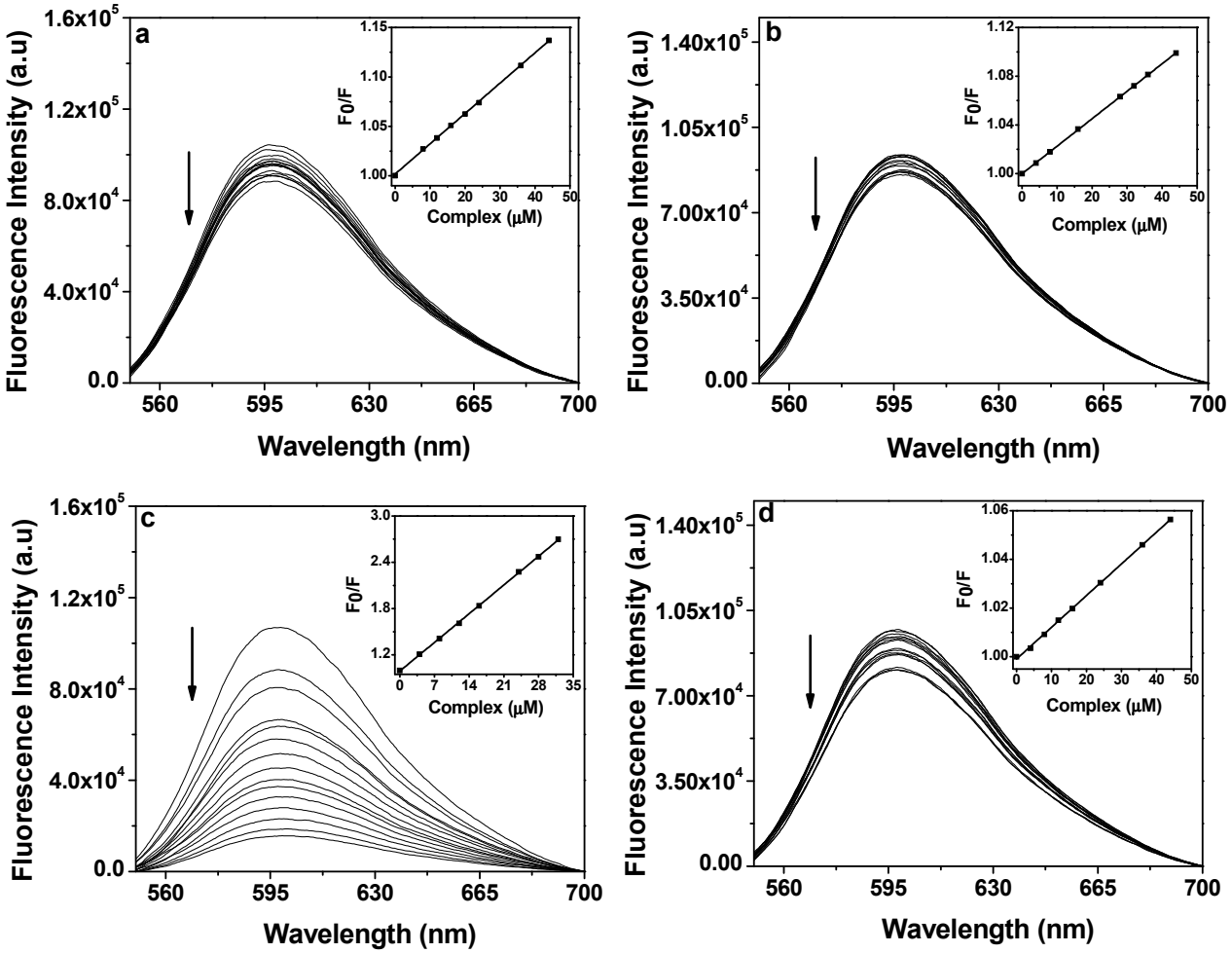

Fig. 9.

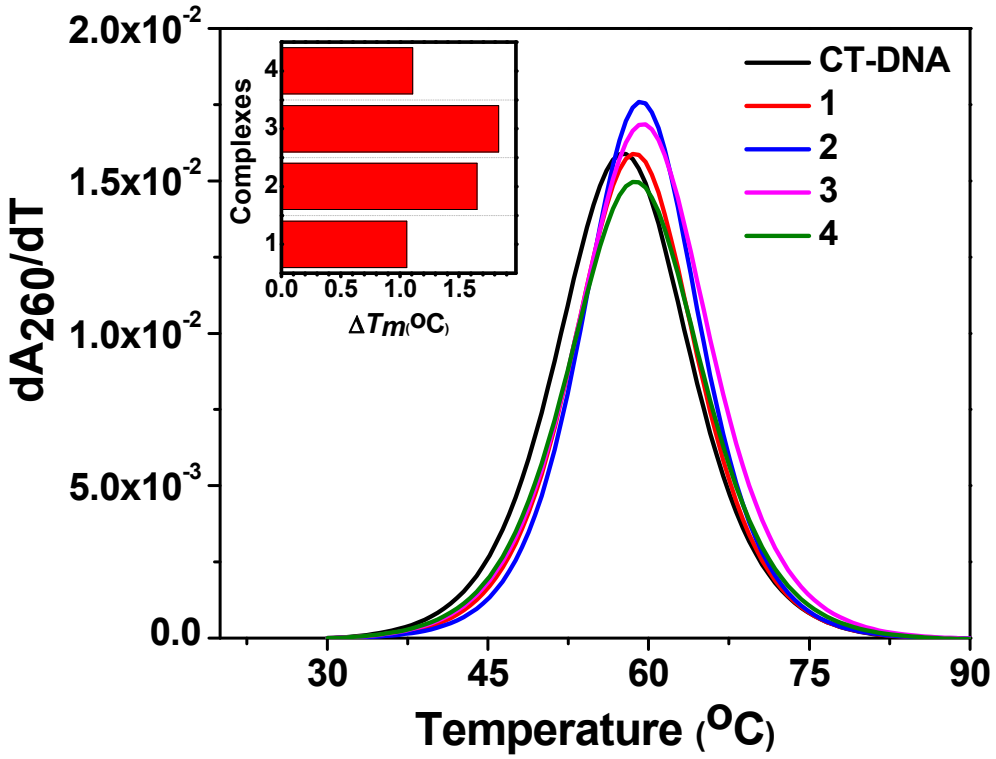

Fig. 10.

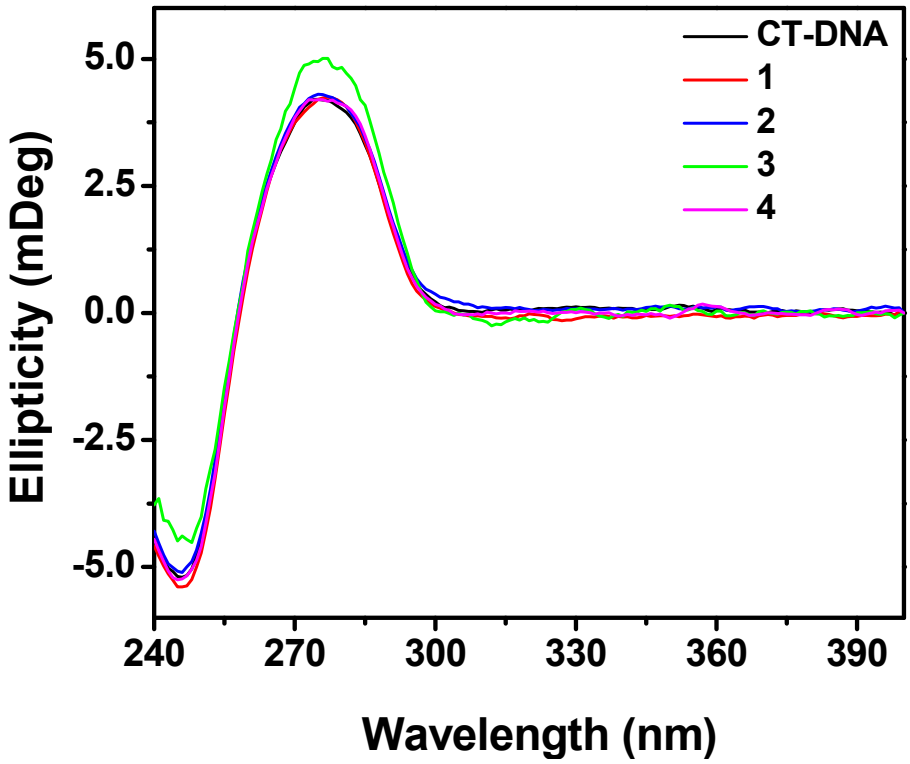

Fig. 11.

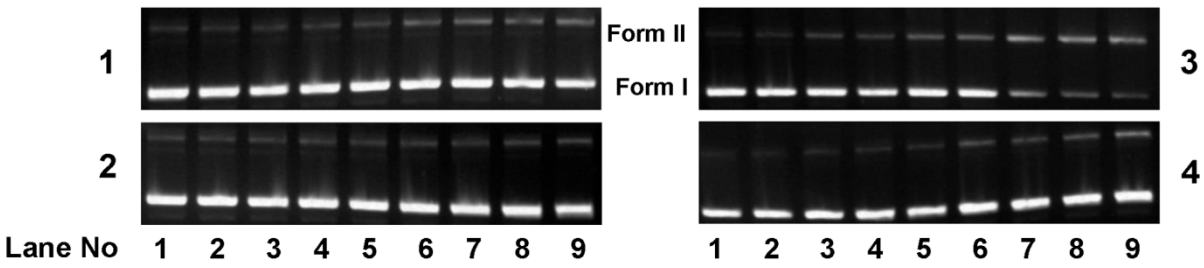

Fig. 12.

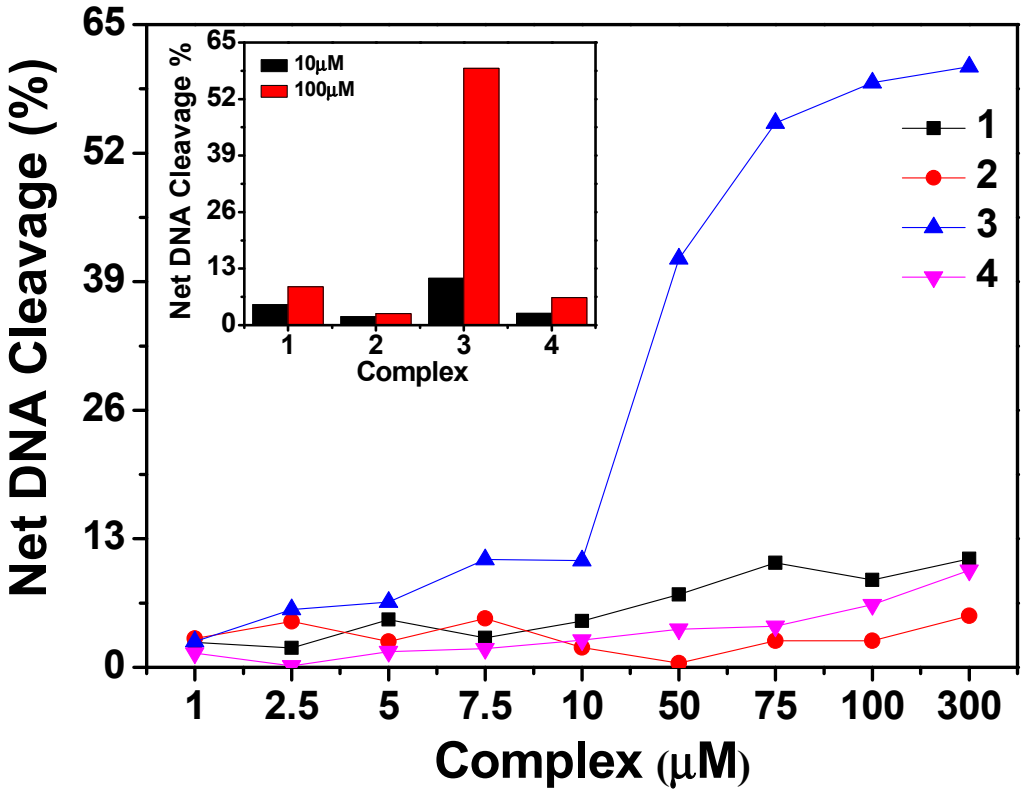

Fig. 13.

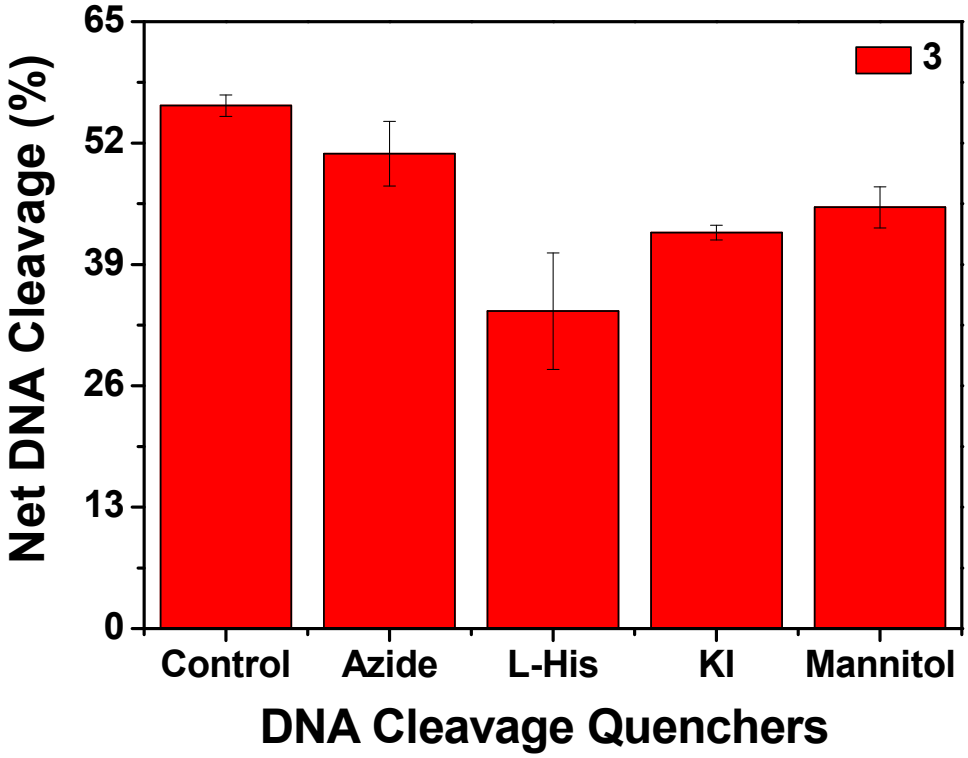

Fig. 14.

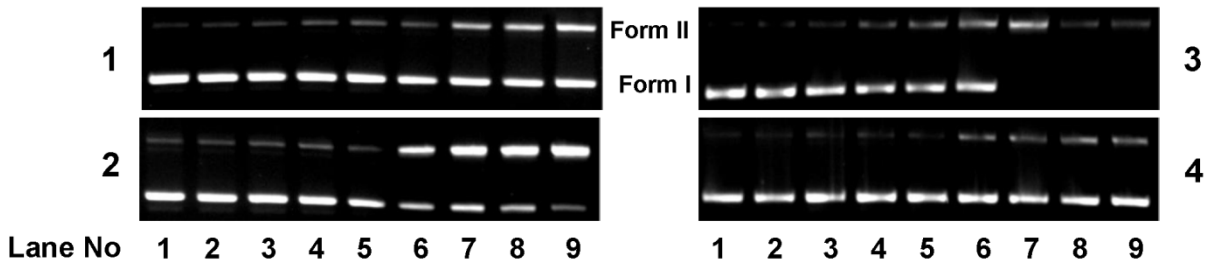

Fig. 15.

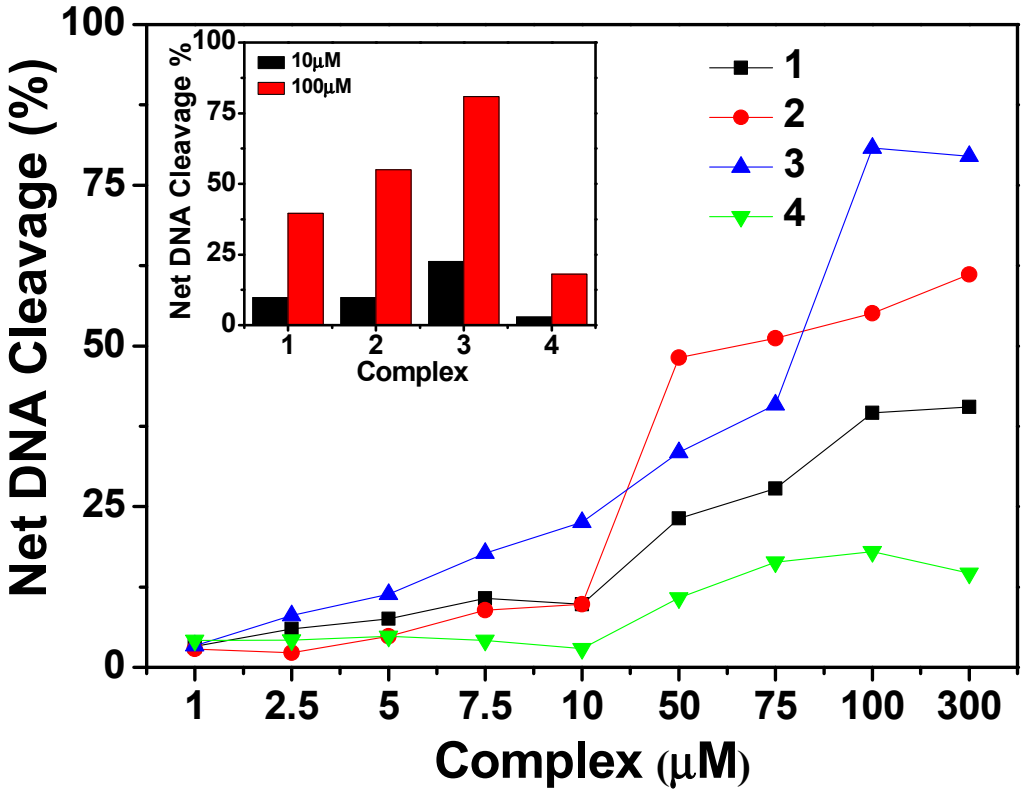

Fig. 16.

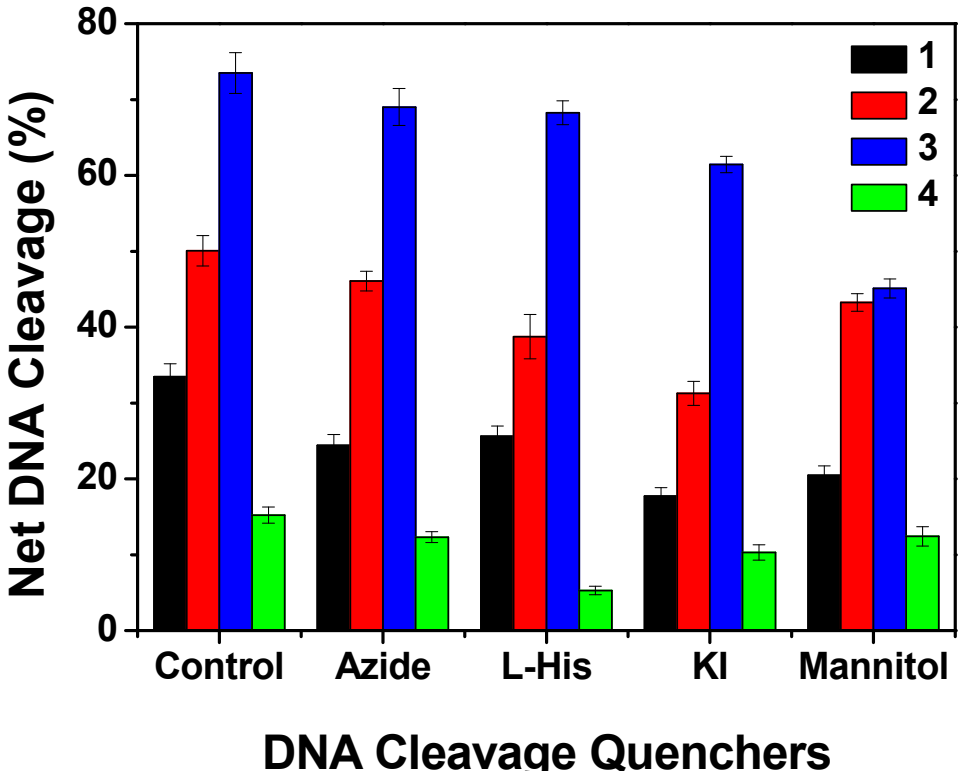

Fig. 17.

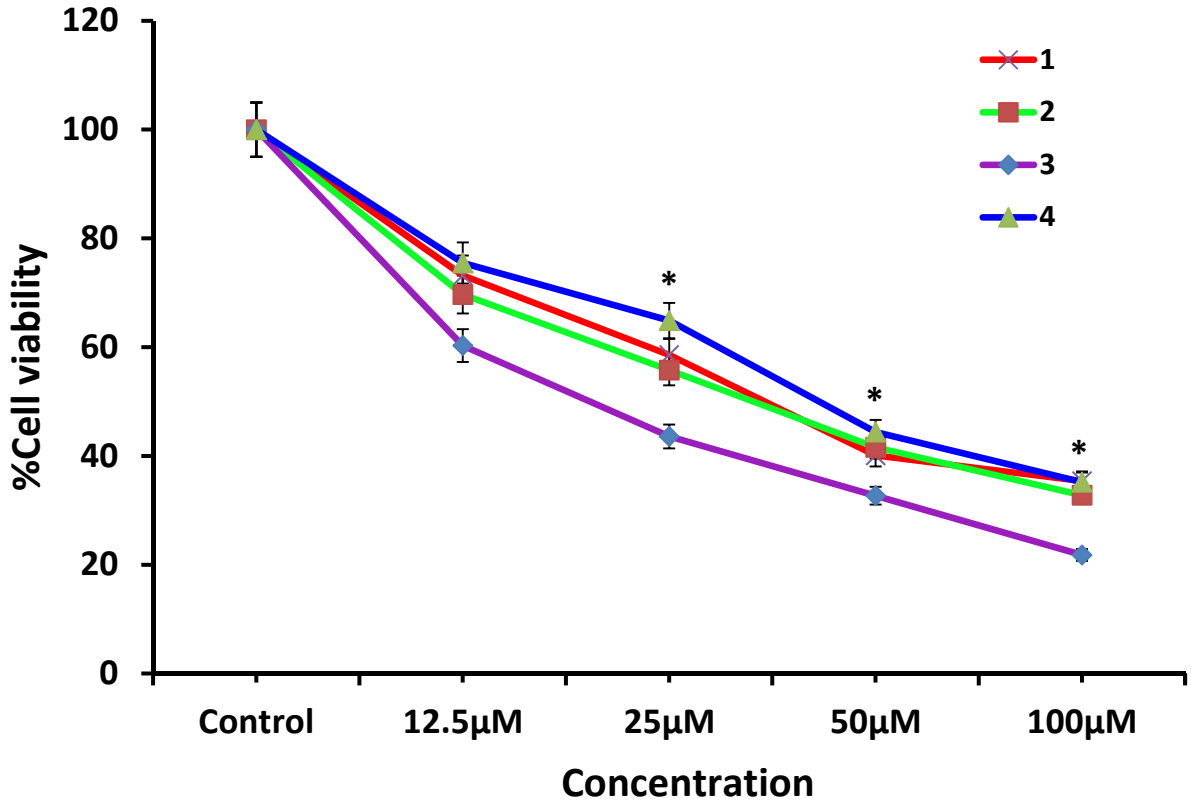

Fig. 18.

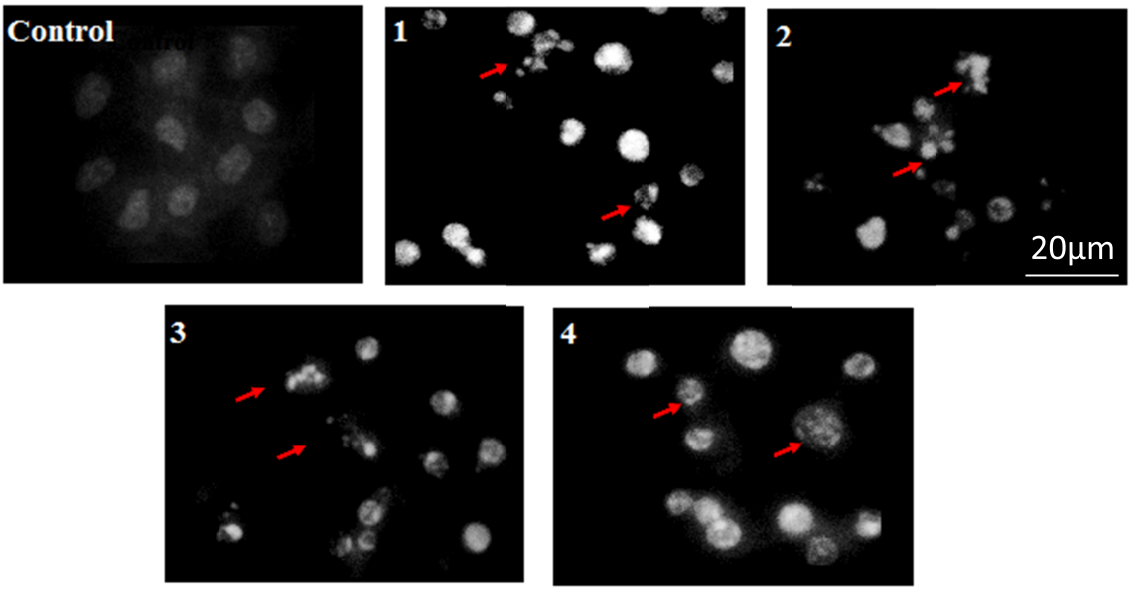

Fig. 19.